

AD-A122 274

MECHANICAL RESPONSE OF MATERIALS WITH PHYSICAL DEFECTS
PART I MODELING OF..(U) LEMIGN UNIV BETHLEHEM PA INST
OF FRACTURE AND SOLID MECHANICS... G C SIM ET AL.

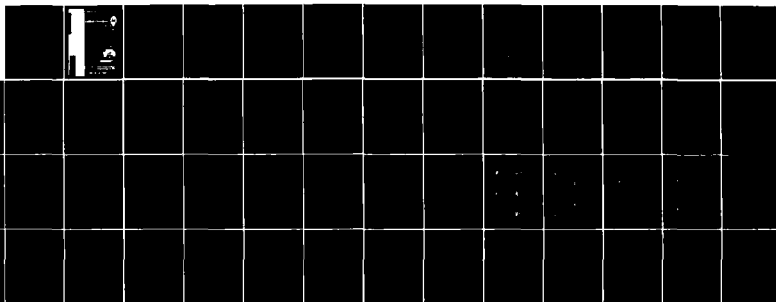
1/1

UNCLASSIFIED

OCT 81 IFSM-81-108 AFOSR-TR-82-1048

F/G 20/11

NL



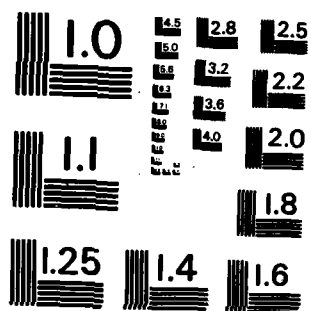
END

DATE

FILED

1983

DT 6



MICROCOPY RESOLUTION TEST CHART
NATIONAL BUREAU OF STANDARDS-1963-A

AD A 122274

ONE FILE COPY

Unclassified

SECURITY CLASSIFICATION OF THIS PAGE (When Data Entered)

REPORT DOCUMENTATION PAGE		READ INSTRUCTIONS BEFORE COMPLETING FORM
1. REPORT NUMBER AFOSR-TR- 82 - 1045	2. GOVT ACCESSION NO. AD-A122 274	3. RECIPIENT'S CATALOG NUMBER
4. TITLE (and Subtitle) Mechanical Response of Materials with Physical Defects. Part 1: Modeling of Material Damage for Center Cracked Panel		5. TYPE OF REPORT & PERIOD COVERED ANNUAL 1 Jan 81 - 30 Sep 81
		6. PERFORMING ORG. REPORT NUMBER IFSM-81-105
7. AUTHOR(s) G. -C. Sih and P. Matic		8. CONTRACT OR GRANT NUMBER(s) F49620-81-K-0005
9. PERFORMING ORGANIZATION NAME AND ADDRESS Institute of Fracture and Solid Mechanics Lehigh University Bethlehem, Pennsylvania 18015		10. PROGRAM ELEMENT, PROJECT, TASK AREA & WORK UNIT NUMBERS 61102F 2307/B1
11. CONTROLLING OFFICE NAME AND ADDRESS Air Force Office of Scientific Research Bolling Air Force Base, D.C. 20332		12. REPORT DATE October 1981
		13. NUMBER OF PAGES 50
14. MONITORING AGENCY NAME & ADDRESS (if different from Controlling Office)		15. SECURITY CLASS. (of this report) Unclassified
		15a. DECLASSIFICATION/DOWNGRADING SCHEDULE
16. DISTRIBUTION STATEMENT (of this Report) Approved for public release; distribution unlimited.		
17. DISTRIBUTION STATEMENT (of the abstract entered in Block 20, if different from Report)		
18. SUPPLEMENTARY NOTES		
19. KEY WORDS (Continue on reverse side if necessary and identify by block number) Accumulated damage Non-linear behavior of cracked panel Strain energy density criterion Material damage ahead of crack Crack growth Finite element		
20. ABSTRACT (Continue on reverse side if necessary and identify by block number) This is the first part of an investigation dealing with the global load-displacement behavior of a stationary center cracked panel in which material damage is accumulated for each increment of loading. The finite element procedure was used where the local stiffness in regions ahead of the crack undergo changes in accordance with a predetermined failure criterion. The resulting non-linear behavior of the load-displacement curves are obtained by two different damage models. Growth of the crack will be considered in the second part of this work.		

DD FORM 1 JAN 75 1473 EDITION OF NOV 65 IS OBSOLETE

Unclassified

SECURITY CLASSIFICATION OF THIS PAGE (When Data Entered)

Unclassified

SECURITY CLASSIFICATION OF THIS PAGE (When Data Entered)

cont

The proposed damage concept models the development of microcracks and/or voids ahead of a macrocrack by altering the local stiffness. As the material elements are damaged, the linearly elastic behavior changes to pseudo-linearly elastic behavior, under the assumption that any energy dissipated due to microcrack generation is no longer recoverable upon unloading. No other dissipative mechanism is assumed.

A Single Damage Level model was based on a "damaged/undamaged" evaluation of each finite element in the panel specimen. The damage threshold was based on the elastic strain energy density at the yield stress level of an uniaxial tensile test specimen. The effect of damage on the bulk material properties in the damage zone were taken to be a reduced secant elastic modulus consistent with the uniaxial tensile test specimen and with the effective elastic properties of the microcracked portion of the medium. The damage status of the element was the independent variable of the model, subject to the failure sequence of all elements determined by the strain energy density ranking of each element. The applied load necessary for a given element to reach the strain energy density value at yield stress was the dependent quantity of the model.

A Multiple Damage Level model incorporated twenty-four discrete values of the secant elastic modulus of a specified uniaxial tensile specimen true stress-true strain curve. The strain energy density level at yield stress was taken to be the damage threshold level. The value of the secant modulus representing the highest level of material damage was chosen to be consistent with the ultimate stress and ultimate strain values of the tensile specimen curve, and the effective elastic properties of the microcracked portion of the medium. The applied load was the independent variable which determined the level of damage in each element of the model for a given load. Note that this is in contrast to the Single Damage Level model, where the reverse was true.

Unclassified

SECURITY CLASSIFICATION OF THIS PAGE (When Data Entered)

AIR FORCE OFFICE OF SCIENTIFIC RESEARCH / AFOSI
NOTICE OF TECHNICAL INFORMATION TO DTIC
This technical report has been reviewed and is
approved for release to the public under E.O. 13526-12.
Distribution is unlimited.
MATTHEW J. KUNNER
Chief, Technical Information Division

MECHANICAL RESPONSE OF MATERIALS WITH PHYSICAL DEFECTS

PART 1: MODELING OF MATERIAL DAMAGE FOR CENTER CRACKED PANEL

by

G. C. Sih and P. Matic

Institute of Fracture and Solid Mechanics

Lehigh University

October 1981



RECEIVED FBI
NTIS GRA&I
DTIC TAB
UNANNOUNCED
JUSTIFICATION
DISTRIBUTION
ANALYSIS
JAN 1968
STATION

ABSTRACT

This is the first part of an investigation dealing with the global load-displacement behavior of a stationary center cracked panel in which material damage is accumulated for each increment of loading. The finite element procedure was used where the local stiffness in regions ahead of the crack undergo changes in accordance with a predetermined failure criterion. The resulting non-linear behavior of the load-displacement curves are obtained by two different damage models. Growth of the crack will be considered in the second part of this work.

The proposed damage concept models the development of microcracks and/or voids ahead of a macrocrack by altering the local stiffness. As the material elements are damaged, the linearly elastic behavior changes to pseudo-linearly elastic behavior, under the assumption that any energy dissipated due to microcrack generation is no longer recoverable upon unloading. No other dissipative mechanism is assumed.

A Single Damage Level model was based on a "damaged/undamaged" evaluation of each finite element in the panel specimen. The damage threshold was based on the elastic strain energy density at the yield stress level of an uniaxial tensile test specimen. The effect of damage on the bulk material properties in the damage zone were taken to be a reduced secant elastic modulus consistent with the uniaxial tensile test specimen and with the effective elastic properties of the microcracked portion of the medium. The damage status of the element was the independent variable of the model, subject to the failure sequence of all elements determined by the strain energy density ranking of each element. The applied load necessary for a given element to reach the strain energy density value at yield stress was the dependent quantity of the model.

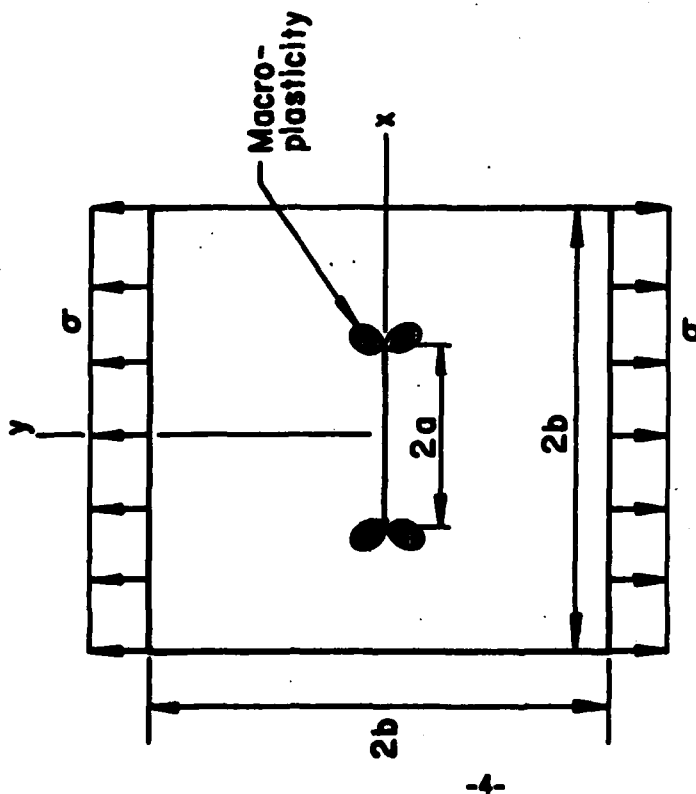
A Multiple Damage Level model incorporated twenty-four discrete values of the secant elastic modulus of a specified uniaxial tensile specimen true stress-true strain curve. The strain energy density level at yield stress was taken to be the damage threshold level. The value of the secant modulus representing the highest level of material damage was chosen to be consistent with the ultimate stress and ultimate strain values of the tensile specimen curve, and the effective elastic properties of the microcracked portion of the medium. The applied load was the independent variable which determined the level of damage in each element of the model for a given load. Note that this is in contrast to the Single Damage Level model, where the reverse was true.

INTRODUCTION

There is increasing concern in the field of continuum mechanics that the interaction between changes in material properties and material behavior, due to damage in the form of microcracks or other defects, is not being distinguished and assessed quantitatively. In recent years, attention has been focused on studying the accumulation of physical defects in the solid as it is being loaded and observing the changes in the state of stresses and strains. This differs fundamentally from the classical formulation of constitutive equations that do not address the physical damage of the material.

In order to develop more realistic constitutive relations that reflect the occurrence of irreversibility caused by physical damage of the loaded material, the behavior of a center cracked panel (Figure 1) under unidirectional tensile loading perpendicular to the crack has been studied in detail. Such a specimen features a macro-defect in the form of a symmetrically located crack, whose length is of the same order of magnitude as the specimen size. Under sufficiently high loads, the macrocrack would be expected to increase in length. For some value of the load, the process will become unstable and result in failure of the panel.

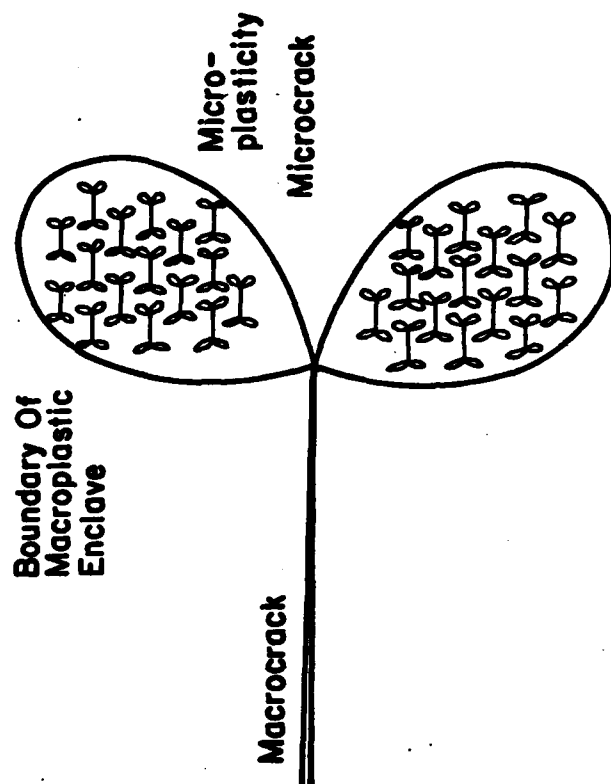
A specimen made of a "ductile" material would be expected to develop damage at a lower scale level in the form of microcracks and/or microvoids. These defects may be initially present in the material, or may coalesce from the movement of dislocations and other defects at an even smaller scale, i.e., the atomic scale. In the presence of a macrocrack, such regions are known to exist ahead of the crack tip on both sides of a two-ended crack. The latter regions, commonly identified as "plastic enclaves" in the classical theory of plasticity, have



Applied Load $p = 2\sigma tb$ $a = 1.5"$

Thickness $t = 1.0"$ $b = 4.0"$

$a/b = 0.375$



Schematic Detail Of Crack Tip In Ductile Material

Figure 1 - Center cracked panel specimen

been the subject of much attention since the dimensions of such regions can be significant when compared to the crack length. The microcracks themselves will produce microplastic regions ahead of both crack tips, also. Their effect on the propagation of the macrocrack is not yet fully understood*.

In order to develop a model of the processes described above, it is assumed that the strain energy density, dW/dV , per unit volume of material, is the quantity that reflects material damage at the micro level, as well as the length and direction of macrocrack propagation at the macro level**. The term "material damage" will refer to processes which utilize strain energy at the continuum scale to produce irreversible changes in the material. These changes will in turn affect the local material behavior as a result of the formation of microcracks, microvoids or coalescence of these defects.

Delameter, Herrmann and Barnett have considered the two dimensional problem of a doubly periodic array of cracks with equal length $2a$. The cracks are parallel to the x-axis and perpendicular to the y-axis. Dislocations have been used to describe the discontinuity in the displacement field which exists across the cracks. The resulting singular integral equations of the first kind have been

* The terminology "small scale yielding" refers to relative size of the plastic enclave as compared with crack length and has caused much confusion when using elastic-plastic solutions of a crack in an infinite medium, i.e., containing no specimen dimensions. It has been shown in [9] and discussed in [13] that the plastic enclaves can be many times greater than the crack length and the state of affairs near the crack is still essentially elastic because the stored elastic energy in an infinite medium ahead of the crack is always much larger than the stored elastic-plastic energy in the enclaves that are finite in dimension. An additional length parameter other than the crack length such as specimen dimension or plate thickness is required for analyzing the influence of plasticity on the global behavior of a specimen or structural component.

** It is considered to be pertinent that the failure criterion at both the micro and macro level be consistent in order to minimize the introduction of arbitrariness into the model.

numerically solved. This formulation accounts for the interaction of the periodic cracks. The effective elastic constants of the medium with elastic modulus E , shear modulus G , and Poisson's ratio ν are calculated on the basis of the strain energy density per unit thickness. In plane strain, the relation for strain energy density is

$$\frac{dW}{dV} = \frac{\sigma_x^2}{2E} + \frac{\sigma_y^2}{2E} - \frac{\nu\sigma_x\sigma_y}{E} + \frac{\tau_{xy}^2}{2G} \quad (1)$$

for a medium in the absence of cracks, and is equated to the relation for a cracked medium,

$$\frac{dW}{dV} = \frac{\sigma_x^2}{2E} + \frac{\sigma_y^2}{2E} - \frac{\nu\sigma_x\sigma_y}{E} + \frac{\tau_{xy}^2}{2G} + \frac{\Delta E}{bd} \quad (2)$$

Here, $\Delta E/bd$ is the energy density change due to one crack in the material, with a spacing between adjacent crack centers of b in the y -direction and d in the x -direction. For a crack subject to Mode I loading,

$$\Delta E_I = \pi\sigma^2a^2(1-\nu^2)B^I/E \quad (3a)$$

while for Mode II loading,

$$\Delta E_{II} = \pi\sigma^2a^2(1-\nu^2)B^{II}/E \quad (3b)$$

where B^I and B^{II} are coefficients which are functions of the distances b and d between cracks. For mixed mode loading, the total energy is given as

$$\Delta E = \Delta E_I + \Delta E_{II}$$

The bulk properties of the cracked medium are orthotropic and calculated to be:

$$E_x = E \quad (4a)$$

$$\nu_{xy} = \nu \quad (4b)$$

$$\frac{E_y}{E} = \frac{\nu_{21}}{\nu} = \frac{1}{1 + (2\pi a^2 B^I / bd)} \quad (4c)$$

$$\frac{G_{xy}}{G} = \frac{1}{1 + (2\pi a^2 B^{II} G / bdE)} \quad (4d)$$

The asymptotic values of E_y and G_{xy} are found to be

$$\lim_{(2a/b) \rightarrow \infty} E_y/E = \frac{1}{1 + \frac{2a}{d}} \quad (5a)$$

and

$$\lim_{(2a/b) \rightarrow \infty} G_{xy}/G = 0 \quad (5b)$$

The first expression implies that a value of E_y/E greater than 0.5 will be the asymptotic value of E_y/E unless the uncracked ligament $d-2a$ between any two collinear cracks becomes as small as the crack periodicity, b , in the y -direction. This is one indication that high crack densities may still result in a significant effective elastic modulus of the bulk material. The shear modulus is reduced significantly by this formulation, to a limiting value of zero.

Gottesman, Hashin and Brull have investigated the upper and lower bounds of the effective properties of a cracked medium using the principals of minimum po-

tential and minimum complementary energy, respectively. For two dimensional plane strain, the change in energy of the total body under uniform loading in the presence of a statistically homogeneous crack distribution will be for m total cracks,

$$\bar{W} = W + \sum_m \Delta W_m = \left(\frac{\sigma_x^2}{2E} + \frac{\sigma_y^2}{2E} - \frac{\nu 12 \sigma_x \sigma_y}{E} + \frac{\tau_{xy}^2}{E} \right) V + \sum_m \Delta W_m \quad (6)$$

where V is the volume of the body and ΔW_m is the energy change associated with each crack. For a crack,

$$\Delta W_m = \frac{1}{2} \sigma_{ij}^0 \int_{S_m} [u_i] n_j ds \quad (7)$$

where $[u_i]$ is the displacement discontinuity across the crack face, S_m is the m th crack surface and n_j is the unit normal to the crack surface. Alternately, in terms of the stress intensity factor, the following expression is obtained:

$$\Delta W_m = (1-\nu^2) \frac{2\pi}{E} \int_0^{a_m} [K_I^2 + K_{II}^2 + (1-\nu)K_{III}^2] dx \quad (8)$$

where a_m is a crack length parameter and K_I , K_{II} and K_{III} are the Mode I, II and III stress intensity factors, respectively.

If the uncracked body is isotropic, and if the crack distribution is statistically isotropic also, then the effective bulk modulus \bar{K} and shear modulus \bar{G} can be expressed in the form

$$\frac{1}{\bar{K}} = \frac{1}{K} + \frac{1}{\Delta K} \quad (9a)$$

and

$$\frac{1}{G} = \frac{1}{G} + \frac{1}{\Delta G} \quad (9b)$$

where the quantities $1/\Delta K$ and $1/\Delta G$ are functions of the displacement discontinuities across the crack surface and the globally applied stress.

For the case of low crack density, the upper bound calculation is performed using the principal of minimum potential energy. This solution does not consider crack interaction. A crack density parameter α , of the form

$$\alpha = \frac{1}{V} \sum_m a_m^2 \quad (10a)$$

for two dimensional problems, and

$$\alpha = \frac{1}{V} \sum_m a_m b_m^2 \quad (10b)$$

for three dimensional problems are introduced, where a_m and b_m are crack dimension parameters. The results for randomly oriented circular cracks are

$$E_{upper} = E/[1 + 16\alpha(1-\nu^2)(10-3\nu)/45(2-\nu)] \quad (11a)$$

$$G_{upper} = G/[1 + 32\alpha(1-\nu)(5-\nu)/45(2-\nu)] \quad (11b)$$

where, for circular cracks of radius a_m

$$\alpha = \frac{1}{V} \sum_m a_m^3 \quad (11c)$$

The lower bounds are formulated in terms of the material properties of the uncracked medium, the crack density parameter α , and crack geometry parameters. This last condition is quite restrictive in calculating lower bounds since it requires information on each crack in the general case of random geometry cracks, i.e.,

$$E_{\text{lower}} = E \int f(\alpha, a_m, b_m, c_m) da_m \quad (12)$$

where a_m , b_m and c_m are crack geometry parameters.

Despite the difficulties inherent in the lower bound formulation, the upper and lower bounds for selected crack geometries are found to be within a few percent of each other in most cases considered. The results found by Delameter, Herrmann and Barnett lie within the predicted upper and lower bounds.

Budiansky, O'Connell and Hoenig have applied the self-consistent procedure to the problem of dry, as well as moisture saturated cracks in an elastic medium. By equating the potential energy $\bar{\phi}$ in a representative volume element of a solid with distributed cracks to the potential energy ϕ in the original material plus the change $\Delta\phi$ due to the cracks, an expression of the form is obtained:

$$-\frac{p^2 V}{2K} = -\frac{p^2 V}{2K} - \frac{p^2}{E} \sum_m a^3 f(\bar{\nu}) \quad (13)$$

where the quantities with the over bar refer to the cracked medium. In equation (13), p is a hydrostatic state of stress, V is the volume of the body, K is the bulk modulus, E is the elastic modulus, ν is Poisson's ratio, and a is a crack length parameter. The function f is a non-dimensional shape factor dependent on

crack geometry^{*}.

For the case of uniaxial tension σ_0 applied to the body,

$$-\frac{s^2V}{2E} = -\frac{s^2V}{2E} - \left[\frac{\sigma^2}{E} \sum_m a^3 f(\bar{\nu}) + \frac{\tau^2}{E} \sum_m a^3 g(\bar{\nu}, \beta) \right] \quad (14)$$

Another non-dimensional function g is introduced in conjunction with the resolved local shear stress τ at the crack edge. The angle β is dependent on the orientation of the cracks. The function f is associated with the resolved local tensile stress σ perpendicular to the crack edge.

The effective elastic modulus \bar{E} , effective bulk modulus \bar{K} , and effective Poisson's ratio $\bar{\nu}$ are assumed to follow the conventional relation

$$\bar{E} = 3\bar{K}(1-2\bar{\nu}) \quad (15)$$

Thus, three equations and three unknowns exist to determine the material constants of the cracked medium. The effective shear modulus \bar{G} can be calculated from these three. Assuming that some knowledge of crack size and geometry is known, in the statistical sense, the summation terms in the potential energy expressions can be replaced by correlated or uncorrelated averages of a , $f(\bar{\nu})$, and $g(\bar{\nu}, \beta)$.

In order to evaluate the functions f and g , the average crack energy is calculated since this is the negative of the potential energy change. The ex-

^{*} Note that the critical assumption made is that the crack behaves as if it lies in the medium influenced by the other cracks. This medium exhibits the effective material properties of the cracked medium. Thus, crack interaction is addressed, but without considering each crack individually.

pression discussed above, equation (8), which utilizes the three stress intensity factors, is used for these calculations. Once this is accomplished for the crack geometries under consideration, the material properties can be calculated using a crack density parameter

$$\epsilon = \frac{2N}{\pi} \left\langle \frac{A^2}{P} \right\rangle \quad (16)$$

where N is the total number of cracks, A is the crack area, P the crack perimeter, and the brackets denote ensemble averaging. This is similar to the one cited by Gottesman, Hashin and Brull, as can be seen for the case of all circular cracks in the medium, for which

$$\epsilon = N \langle a^3 \rangle \quad (17)$$

The self-consistent method, interestingly enough, predicts a value of $\epsilon \rightarrow 9/16$ which results in $\bar{\nu} \rightarrow 0$, which is shown to imply \bar{E}/E and $\bar{K}/K \rightarrow 0$. Thus, while not a rigorous criteria for material failure, this value of ϵ could be interpreted as corresponding to a condition of instability in the material based on crack size and population.

For all values of $0 \leq \nu \leq 0.5$, the material properties are found to be preserved to at least 40% of their original value if ϵ does not exceed 0.2. This is for the case of dry (moisture unsaturated) randomly distributed circular cracks.

The behavior of a medium with a distribution of cracks can be formulated in terms of what Eimer has labelled as pseudo-linear elasticity. Recall that a defect free medium is linearly elastic if it is *positively homogeneous*, i.e.,

$$k\sigma_{ij}(\epsilon_{ij}) = \sigma_{ij}(k\epsilon_{ij}) \quad k>0 \quad (18a)$$

and, moreover, *additive*, i.e.,

$$\sigma_{ij}[\epsilon_{ij}^{(1)} + \epsilon_{ij}^{(2)}] = \sigma_{ij}[\epsilon_{ij}^{(1)}] + \sigma_{ij}[\epsilon_{ij}^{(2)}] \quad (18b)$$

where the superscripts 1 and 2 denote arbitrary admissible strain fields for a given body and boundary conditions. If the medium contains defects such as microcracks, the additive condition may be assumed to be violated. This violation is consistent with the introduction of an $\epsilon_{ij}^{(1)}$ strain field which opens the cracks in a portion of the body, followed by the superposition of a strain field $\epsilon_{ij}^{(2)}$ which would close some or all of the cracks which were open. If the condition of positive homogeneity is retained (implying that open cracks would remain open and closed cracks would remain closed upon amplification or attenuation of ϵ_{ij} by a positive factor k), the material behaves in a pseudo-linear fashion. The crack closure process is considered reversible on the assumption that no tangential forces develop during closure. The material behavior is thus reversible upon unloading from both tensile and compressive stress fields. Only microcrack propagation may be assumed to dissipate elastic energy since the material itself is by definition linear.

In this investigation, the results for a center cracked panel specimen in the absence of macrocrack propagation are presented. Macrocrack growth is being considered and will be reported separately. The Strain Energy Density Theory of fracture, as proposed by Sih [12,13] will be used to predict macrocrack growth in conjunction with the microdamage models to be discussed below. This approach to the problem separates the effects of micro and macrodamage. By comparing these

results with the combined effects of damage at both levels, understanding is gained as to which level of damage predominates the specimen global failure process for different structural materials.

The primary concerns in this investigation have been (1) the influence of damage on effective material properties, and the relation of this to (2) the global specimen behavior. Not directly addressed at this point, but of parallel concern, are the means by which the effective properties of a material in both the virgin and damaged states are obtained experimentally. These and subsequent analyses should provide greater understanding of the relation of tensile test specimen data to global structural behavior.

DAMAGE MODELS AND FINITE ELEMENT FORMULATION

Generally speaking, material nonlinearity* exhibited on the stress-strain curve for metals implies irreversibility due to material damage. This being inherently a path dependent process is sensitive to the rate of loading as each increment of load increase will affect the stress and strain state which in turn governs the next increment of material damage. Hence, nonlinear stress and failure analysis cannot be analyzed independently as in the linear case and must be considered in sequence within each increment of loading. Failure to do so results in unphysical and unrealistic prediction.

All stress analysis used to generate the load-displacement curves were carried out on the center cracked panel specimen for a material with characteristics of a low yield stress ($\sigma_y = 35,000$ psi) structural steel. The load-displacement curves were calculated incrementally in a series of "stress analysis-material damage assessment" increments or cycles.

The Axisymmetric/Planar Elastic Structures (APES) two-dimensional fracture mechanics and stress analysis finite element program [8] performed the stress analyses portion of each increment. The formulation of APES utilizes quad-12 elements which allow for cubic displacement fields and quadratic stress and strain fields within each element. The $r^{1/2}$ displacement field in the immediate vicinity of the crack tip is embedded in the solution through the use of $1/9$ to $4/9$ nodal spacing on the element sides adjacent to the crack tip. The tensile loading of the panel subjects the crack to a symmetric Mode I situation, thus requiring only one quarter of the physical problem (Figure 2) to be modelled by

* Global and local nonlinearity should be distinguished. The present analysis assumes linearity for the undamaged material while nonlinear response is developed globally for each increment of loading.

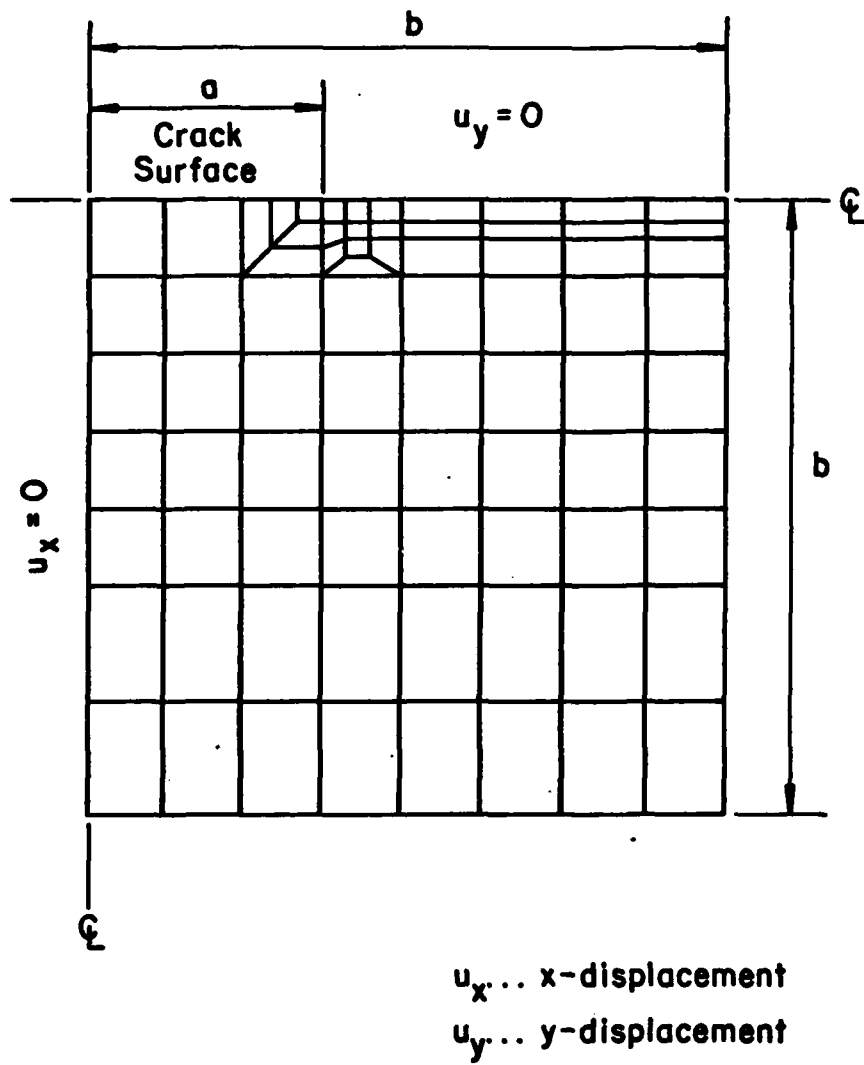


Figure 2 - Finite element grid

440 nodes which define 77 elements. The CDC 6400 computer used in this study typically required 225 system seconds and 132k of central memory to complete the stress analysis for a given specimen load and damage distribution.

The damage processes that occur in the material manifest themselves by changes in the material properties at the continuum level. The finite element formulation allows for this by associating with each element one of up to 25 different material property pairs (i.e., elastic modulus E , and Poisson's ratio ν). Thus, a set of properties (E_1, ν_1) corresponding to the initial elastic behavior of the material, as defined from an uniaxial tensile test specimen, and up to 24 discrete material property pairs (E_i, ν_i) for $i = 2, 3, 4, \dots, 24$, different instances in the damaged material's developing history.

Two distinct types of material damage models were used to generate load-displacement curves for the center cracked specimen. The exact type of damage which accumulates in the material, i.e., the microcrack sizes and shapes, has not been specified in detail. Rather, reasonable lower bounds on the effective properties of the damaged material have been used to generate the bulk behavior of cracked elastic media. The type of damage producing this bulk behavior obviously is not unique, in the sense that a wide variety of crack distributions, geometries, sizes, and orientation can result in the same behavior of the cracked media. The rate of loading can also alter the bulk behavior.

The first type of model provided one of two conditions for each element in the center cracked panel specimen, i.e., either "undamaged" or "damaged". This simple model is interesting in two respects. First, the single level of damage reduces the complexity of the developing damage zone. This allows the effect of damage in a single region (or element in this case) to be directly evaluated

without additional changes in material properties in other regions of the panel specimen. Second, the damage process is considered* as a sequence of "events", i.e., changes in element material properties from the undamaged to the damaged states. Thus, the damage process is discretized to one element at a time.

The damage in the panel specimen was assessed in the method outlined below. After each stress analysis of the center cracked panel, the undamaged elements were ordered in terms of decreasing average strain energy density. Ideally, each element experiencing damage would specify an applied load increment, thus producing the unique element damage sequence and load-displacement curve for each panel specimen. Due to constraints on computing, however, multiple element damage was used to generate the load increment subject to the upper and lower bounding criteria for the load increments discussed in Appendix A. By incrementing the damage of the elements beyond the initial increment in groups typically no longer than five elements per increment, load displacement curves consistent with the damage model and bounding procedures were obtained. The change $\Delta S/V_i$ in panel stiffness S per the i th damaged element volume V_i was small when compared to the overall panel stiffness value. In the event that the damage region of the previous increment enhanced the dW/dV value of an undamaged element to a value indicating failure at the prior load, the failure of such an element could be incorporated into the next damage increment with a negligible effect on the overall characteristics of the load-displacement curve.

Two analyses of the center cracked panel were performed using the Single Damage Level model. In both cases, the strain energy density at the yield stress, $(dW/dV)_{ys} = \sigma_y^2/2E$, of a uniaxial tensile specimen was used as the criterion by

*To the ordinary mind, the material damage is a discrete process for the simple reason that continuity cannot be conceived physically but only in the limit as a mathematical process.

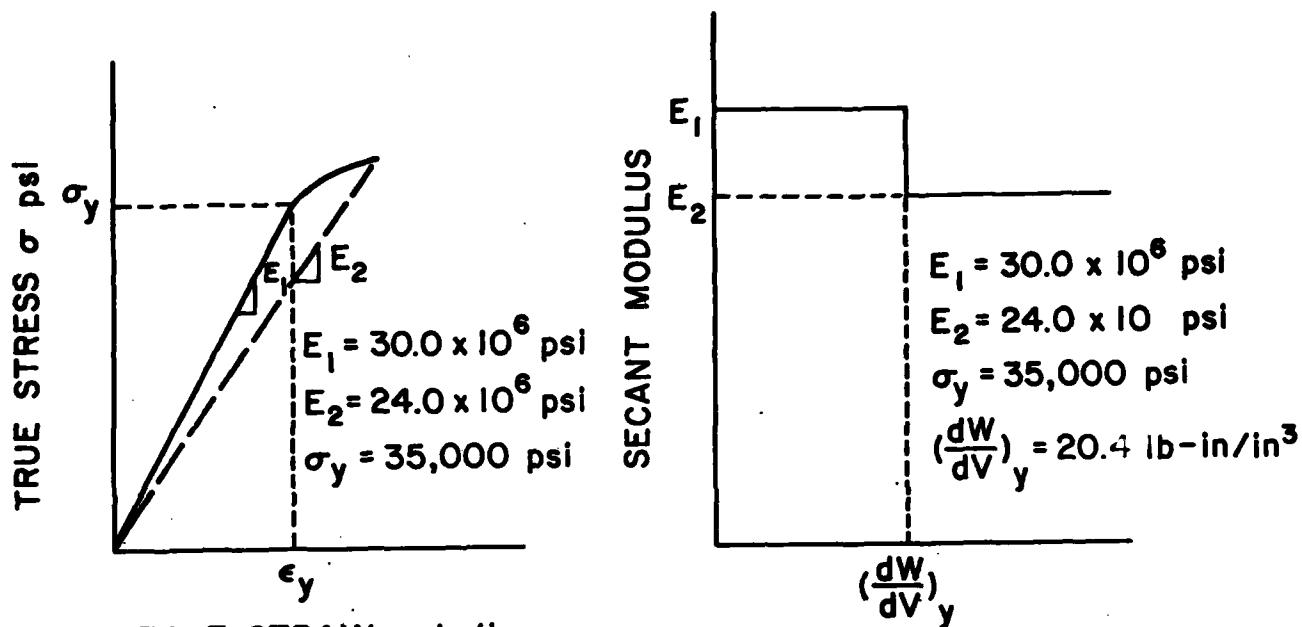
which the damage process would occur in the material. This is consistent with the assumption that the nonlinear behavior of the tensile specimen coincides with the onset of elastic energy dissipation to damage processes. The damage status of the i th element is determined according to the following

$$\left(\frac{dW}{dV}\right)_i \leq \left(\frac{dW}{dV}\right)_{ys} \quad \text{Undamaged Material} \quad (19a)$$

$$\left(\frac{dW}{dV}\right)_i > \left(\frac{dW}{dV}\right)_{ys} \quad \text{Damaged Material} \quad (19b)$$

In the first application of the model, the damaged material elastic modulus was assumed to be a factor of 0.8 times the undamaged modulus obtained from the uniaxial tensile specimen (Figure 3). For the second application of the model, the damaged material elastic modulus was taken to be a factor of 0.6 times the undamaged modulus (Figure 4). Since crack propagation is not addressed in these analyses, the exact form of the material's true stress-true strain curve (Figures 3,4) is rather arbitrary beyond the yield point. This is due to the independence of the microdamage model on the critical strain energy density, $(dW/dV)_{cr}$, which is attained at fracture of the tensile specimen.

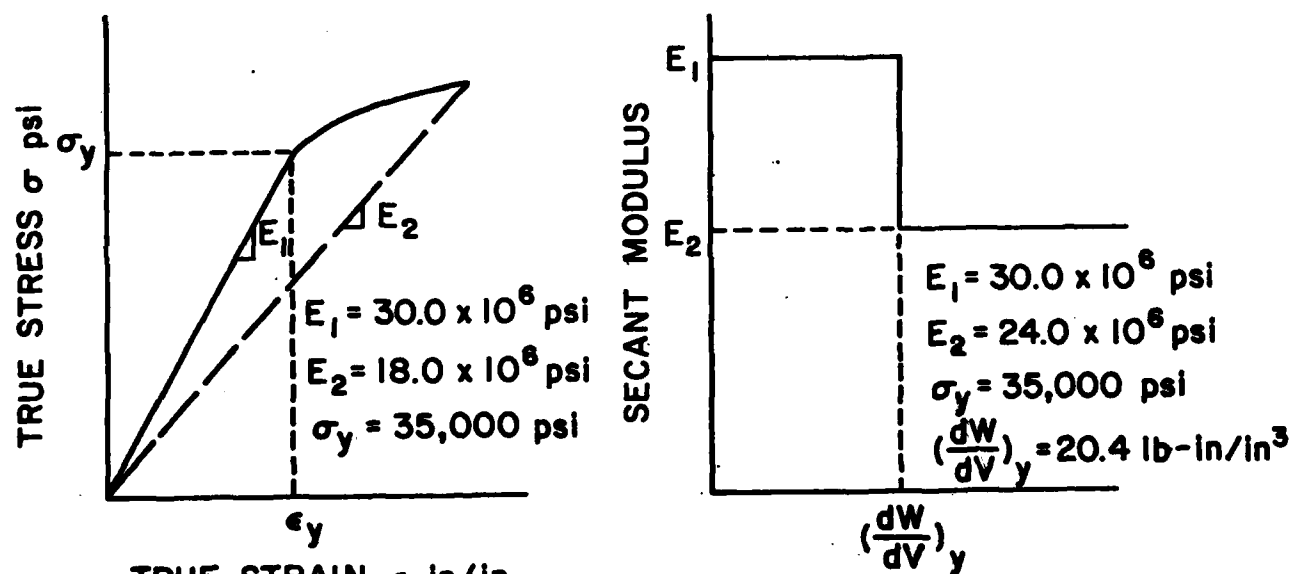
The second damage model used to generate a load-displacement curve for the center cracked panel specimen was based on 24 discrete damage levels (Figure 5) of the virgin material. (Recall that 25 different materials can be incorporated into the finite element formulation). This model will be referred to as the Multiple Damage Level Model. The 24 damage levels were defined on the basis of equal multiple elastic secant modulus reductions. The 24th is defined from the ultimate stress and strain, σ_u and ϵ_u , of the true stress-true strain curve. Since each of the 24 damage levels is attained at a different value of strain energy density, the true stress-true strain curve must be explicitly given (Figure



TRUE STRAIN ϵ in/in

STRAIN ENERGY DENSITY

Figure 3 - Single damage level model No. 1 uniaxial tensile specimen



TRUE STRAIN ϵ in/in

STRAIN ENERGY DENSITY

Figure 4 - Single damage level model No. 2 uniaxial tensile specimen

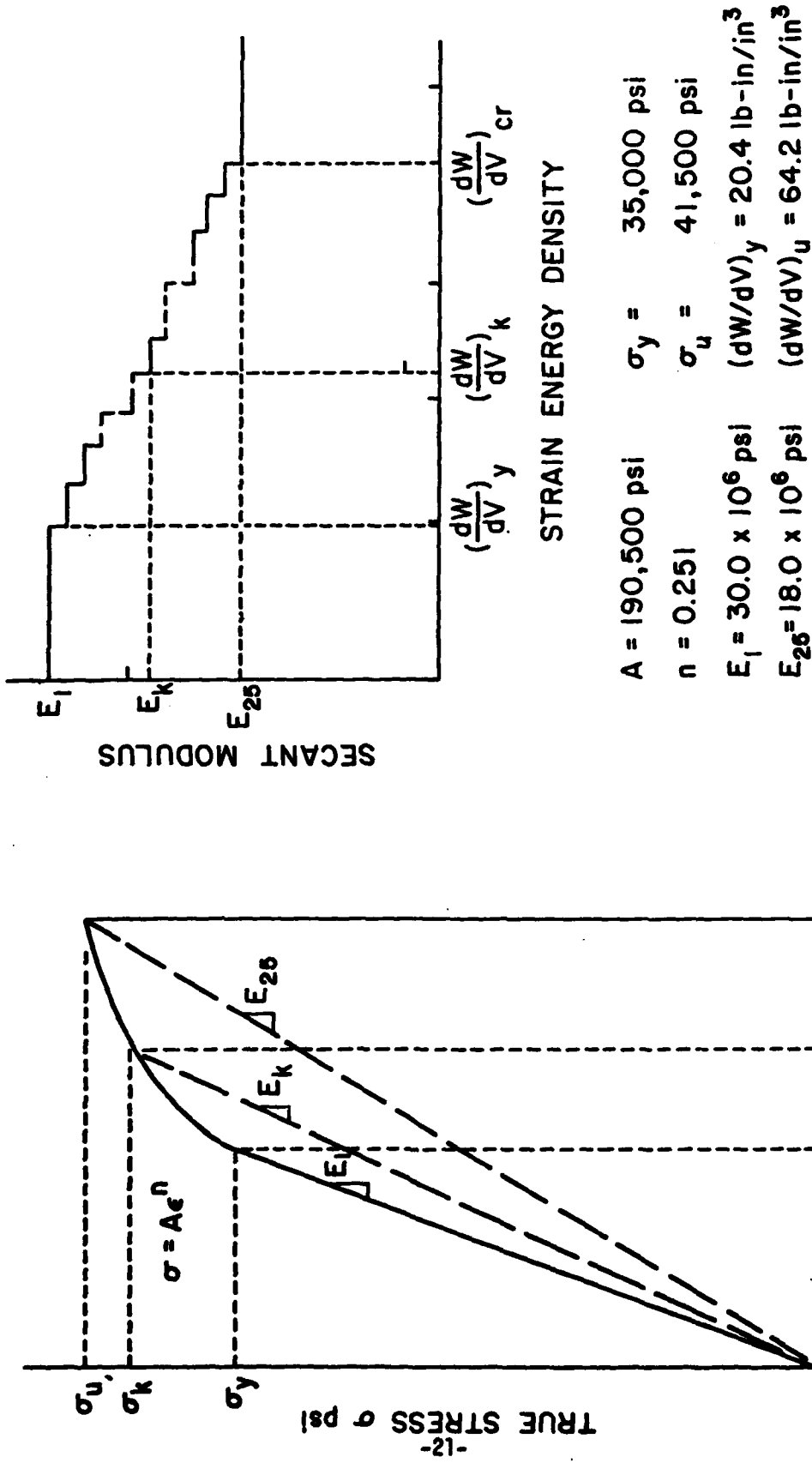


Figure 5 - Multiple damage level model uniaxial tensile specimen

5). For this analysis, the form used was

$$\sigma = A\epsilon^n \quad (20a)$$

The constants were evaluated for a structural steel with the following properties:

Undamaged Modulus	$E_1 = 30.0 \times 10^6$ psi
Yield Stress	$\sigma_y = 35,000$ psi
Ultimate Stress	$\sigma_u = 41,500$ psi
Ultimate Strain	$\epsilon_u = 0.0023$

For this material, the stress-strain relation is

$$\sigma = 190500 \epsilon^{0.251} \quad (20b)$$

For the onset of damage in the material, the strain energy density in the i th element must be

$$\left(\frac{dW}{dV}\right)_i > \left(\frac{dW}{dV}\right)_{ys} \quad (21)$$

For the k th level of damage in the material, characterized by an elastic modulus of E_k , the strain energy density in the i th element must be

$$\left(\frac{dW}{dV}\right)_k < \left(\frac{dW}{dV}\right)_i \leq \left(\frac{dW}{dV}\right)_{k+1} \quad (22)$$

where, for the form of the given stress-strain relation

$$\begin{aligned}
\left(\frac{dW}{dV}\right)_k &= \int_0^{\epsilon_k} \sigma d\epsilon = \int_0^{\epsilon_y} \sigma d\epsilon + \int_{\epsilon_y}^{\epsilon_k} \sigma d\epsilon \\
&= \left(\frac{dW}{dV}\right)_{ys} + \frac{A}{n+1} (\epsilon_k^{n+1} - \epsilon_{ys}^{n+1}) \\
&= \frac{1}{2} \frac{\sigma_y^2}{E_1} + \frac{A}{n+1} (\epsilon_k^{n+1} - \epsilon_{ys}^{n+1})
\end{aligned} \tag{23}$$

The load P is the independent variable in this model, since all elements have the potential to sustain damage at a given load. The increment of the load P can be arbitrarily chosen within the limits of upper and lower bounds (See Appendix A). This is in contrast to the Single Damage Level model, where the damage level is the independent quantity governing the applied load (Figures 6 and 7).

The concept of the mean damage level \bar{d} and damage center (\bar{x}_d, \bar{y}_d) have been introduced in order to quantify the damage zone in terms of a scalar magnitude and its position in the panel specimen. The mean damage level \bar{d} is defined on the basis of the discrete reductions in elastic modulus. Defining the damage in the i th element as the fractional reduction in the elastic modulus by

$$d_i = \frac{E_1 - E_k}{E_1} \tag{24}$$

The mean damage level \bar{d} is calculated as

$$\bar{d} = \frac{1}{V_1} \sum d_i V_i \tag{25}$$

Elements which have not reached the $(dW/dV)_y$ damage threshold, of course, have values of d_i equal to zero. The coordinates (\bar{x}_d, \bar{y}_d) of the damage center are de-

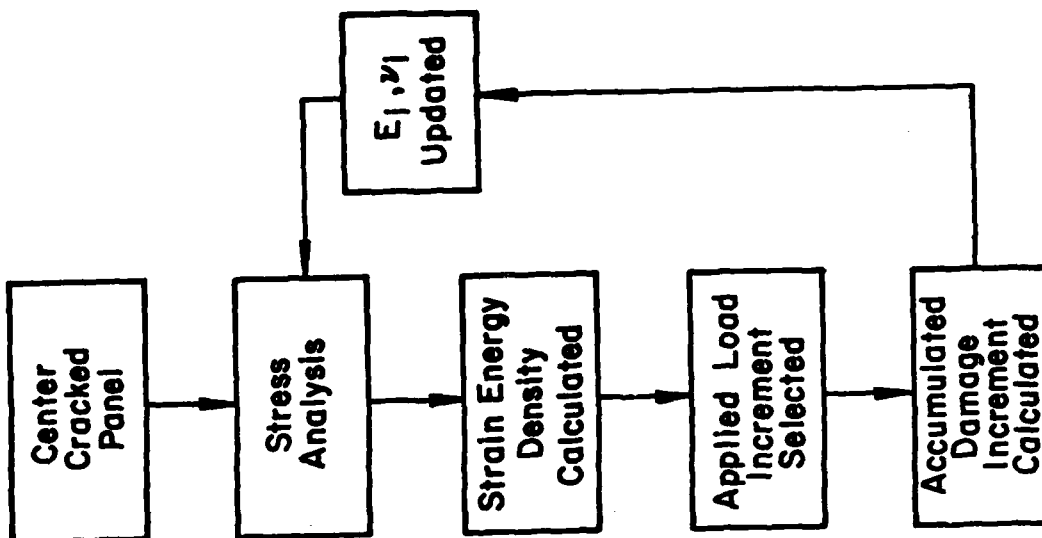


Figure 7 - Multiple damage level model

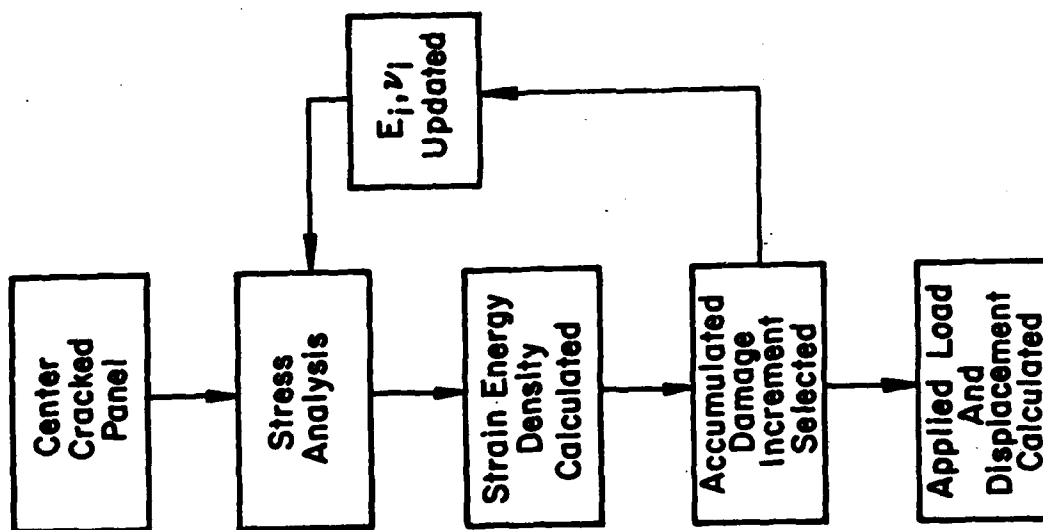


Figure 6 - Single damage level model

defined on the basis of the first moment of the damage distribution

$$\bar{x}_d = \frac{1}{\sum d_i V_i} \sum \bar{x}_i d_i V_i \quad (26a)$$

$$\bar{y}_d = \frac{1}{\sum d_i V_i} \sum \bar{y}_i d_i V_i \quad i = 1, 2, \dots, n_d \quad (26b)$$

where n_d is the number of elements having damage at the applied load. This is simply the discretized form of first moment integrals with the density function taken to be the damage level. The \bar{x}_i and \bar{y}_i coordinates are the coordinates of the i th element centroid.

The locus of the damage center coordinates at each load serves as an indication of how the material damage, as defined by the models incorporated here, is being distributed in the center cracked panel. The crack tip is the origin of the locus of points, and the subsequent curve is indicative as to whether the lower levels of damage at the periphery of the damage zone, or the higher levels nearer to the crack tip are predominating the damage accumulation process at a given load increment. Also, the effect of the free boundary ahead of the crack can be evaluated as to its ability to influence the damage zone's direction of propagation. Typically, one would expect the damage zone boundary to propagate more toward the free surface as the zone size becomes significant with respect to the uncracked ligament length.

LOAD-DISPLACEMENT RESPONSE

Two load-displacement curves are given that were generated from the Single Damage Level model (Figures 8 and 9). The application of these models, with "damaged" modulus values of 0.8 and 0.6 times the undamaged modulus respectively, results in decreasing stiffness values of the center cracked panel (Figure 11). Qualitatively, the nonlinear global behavior of the panel specimen has been recovered by the application of a simplified model accounting for material damage in the form of microcracks.

One load-displacement curve is given which was generated from the Multiple Damage Level model (Figure 10). Recall that the 25th set of material properties of the Multiple Damage Level model are identical to those of the damaged material properties used in the second case of the Single Damage Level model. A comparison of this nonlinear curve to those already mentioned shows that the Multiple Damage Level model results in a load-displacement curve and panel stiffness similar to the first Single Damage Level model. This is to be expected since the mean secant elastic modulus in the damage zone is found to be between 2.5×10^7 and 2.6×10^7 psi, greater than either case of the single level model but closer to the first Single Damage Level model (Figure 12). This indicates that both models, one based on damage increments and one on load increments, are capable of producing reasonable global response estimates of the panel specimen response to applied loads.

The propagation of the damage zones (Figures 13,14,15) is seen to be somewhat different in each of the cases considered. The shape of the damage zones for the Single Damage Level models shows significantly more damage directly ahead of the crack for the second case. This fact, which results in a smaller undamaged

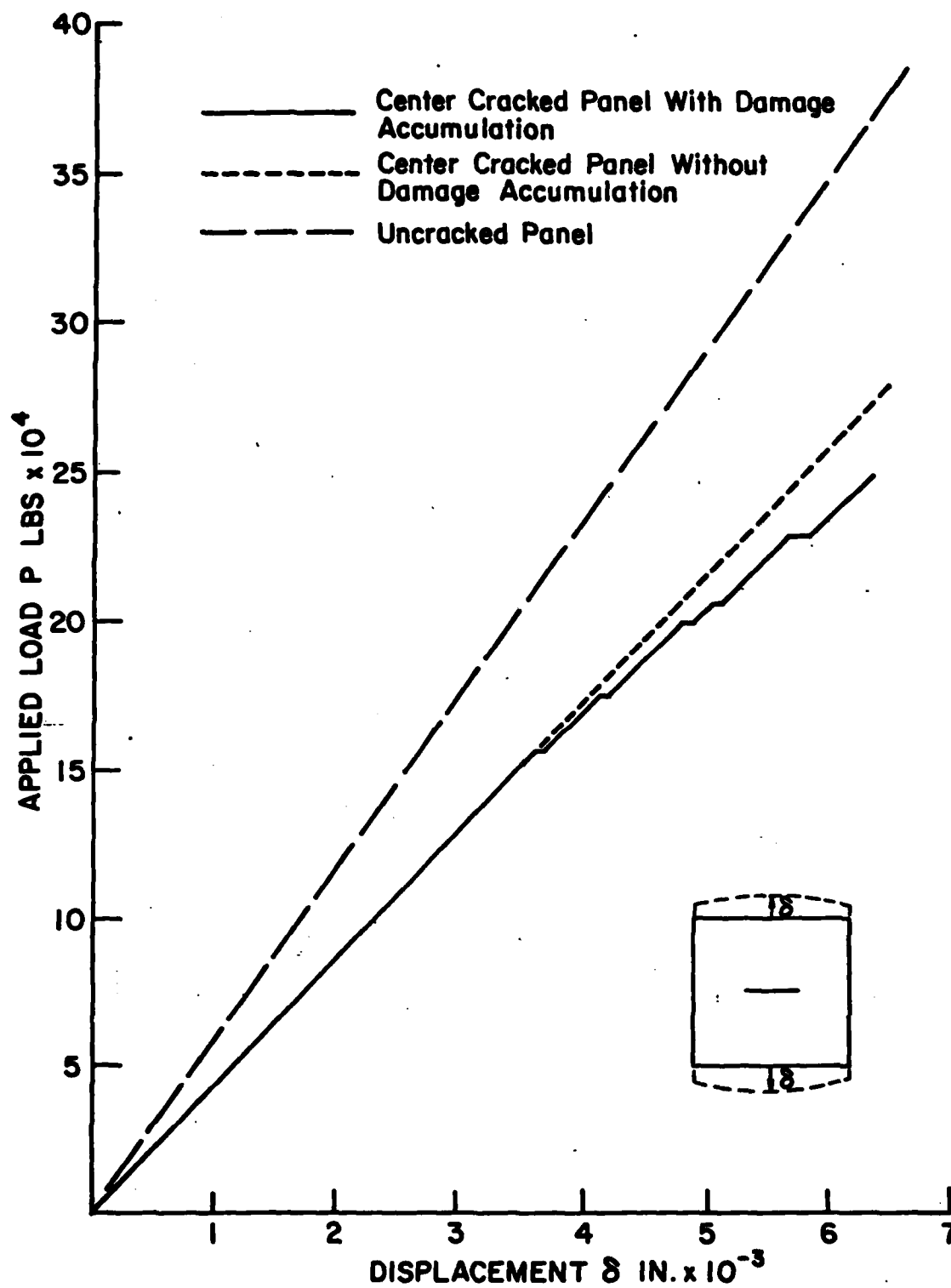


Figure 8 - Single damage level model No. 1 load-displacement curve

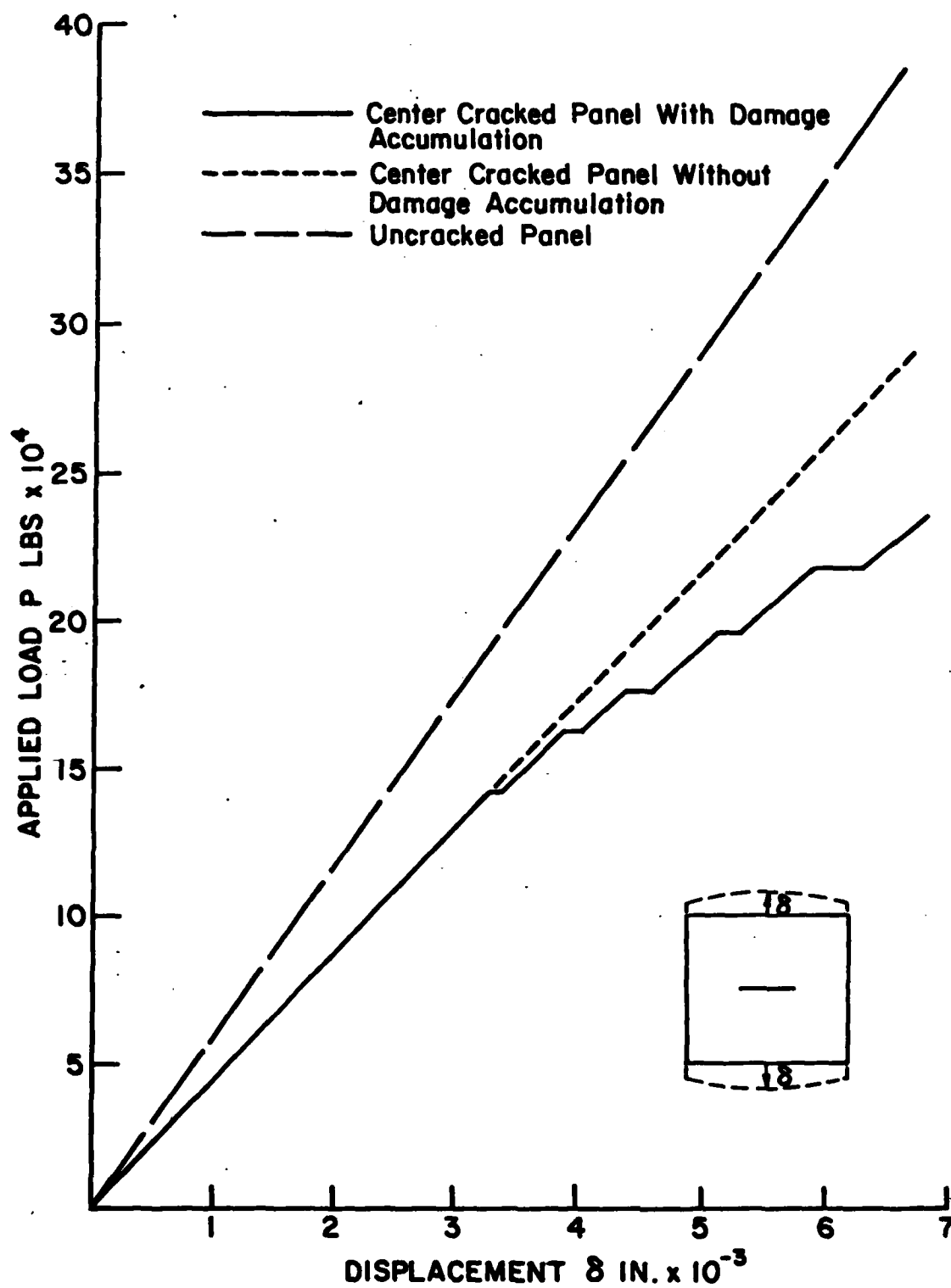


Figure 9 - Single damage level model No. 2 load-displacement curve

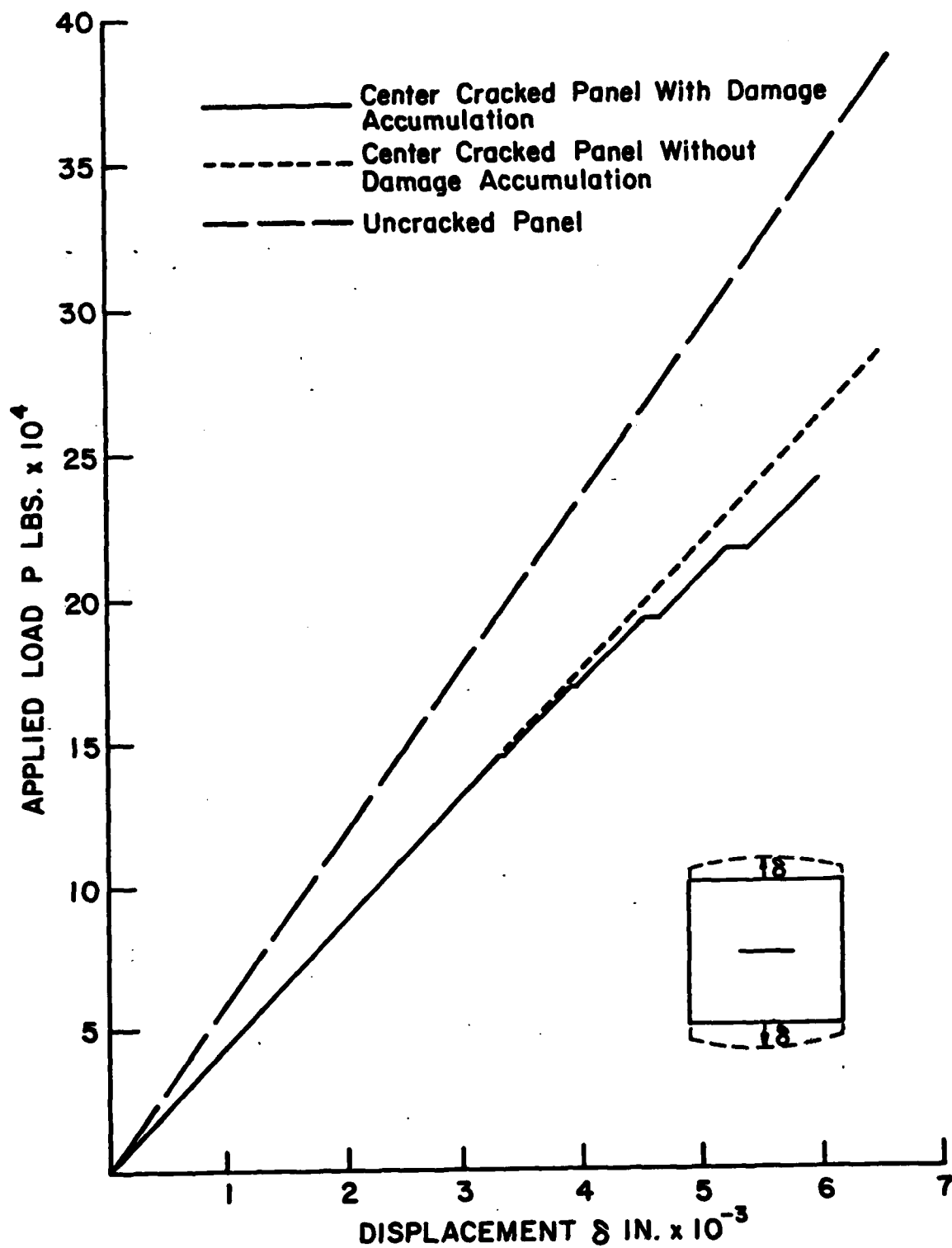


Figure 10 - Multiple damage level model load-displacement curve

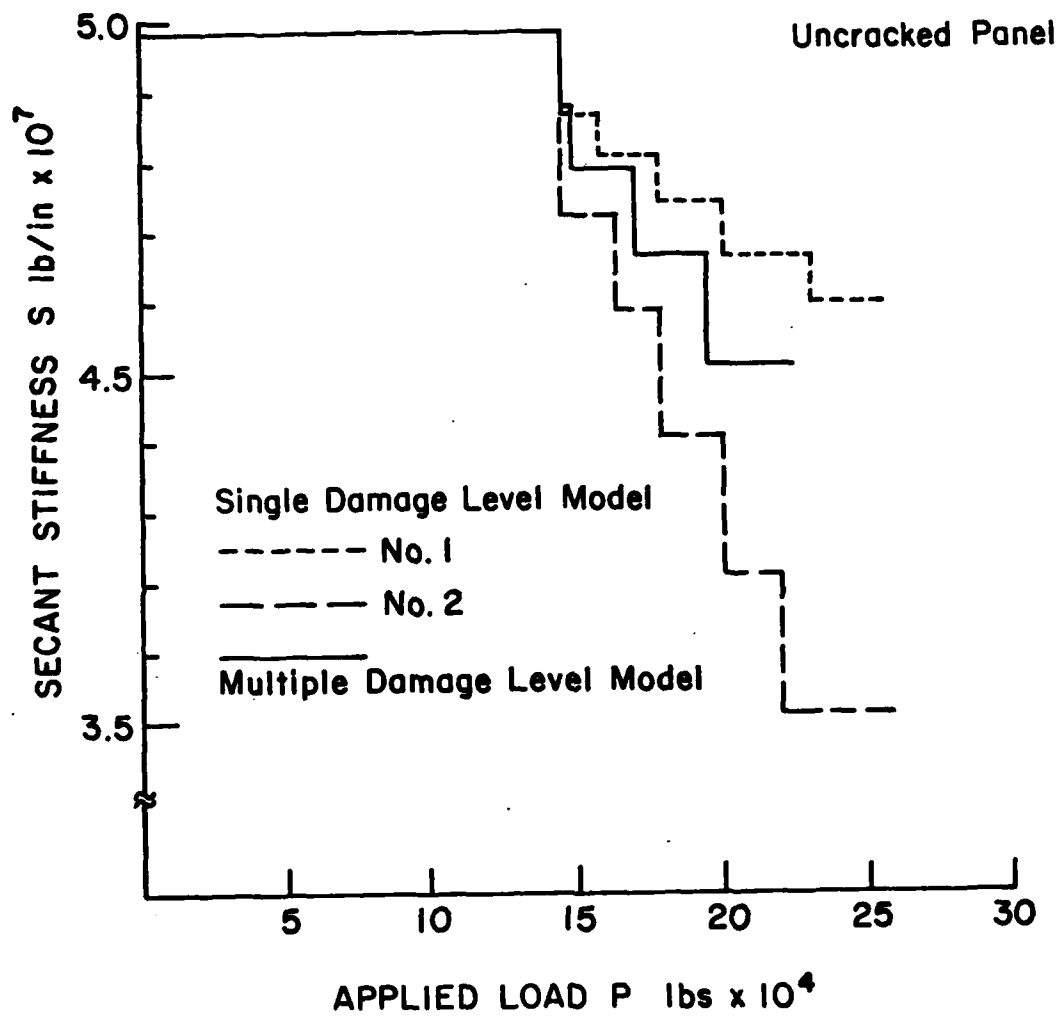


Figure 11 - Center cracked panel secant stiffness versus applied load

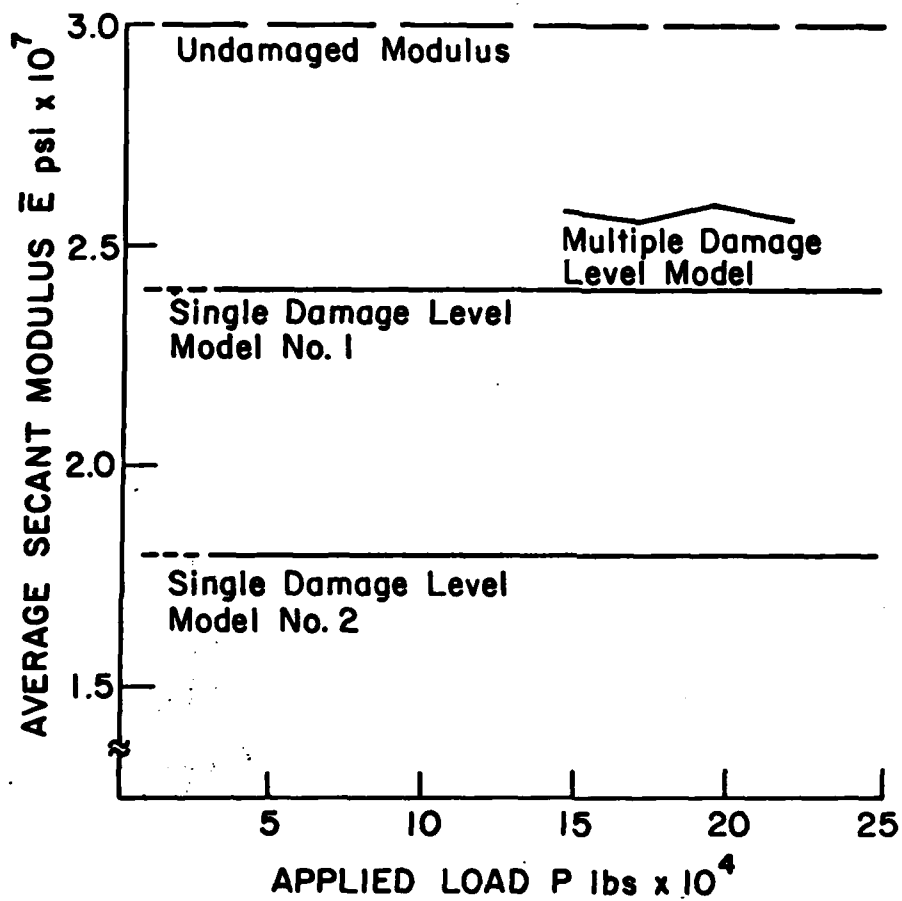
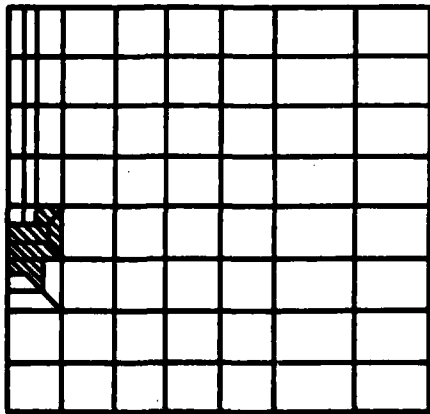
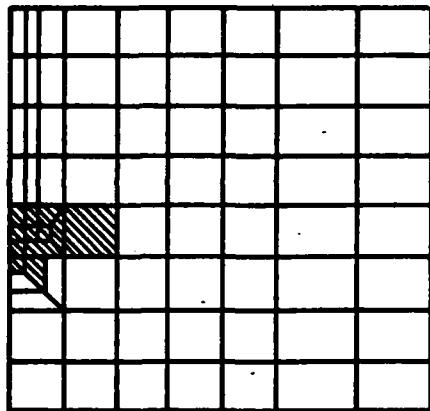


Figure 12 - Average secant modulus versus applied load

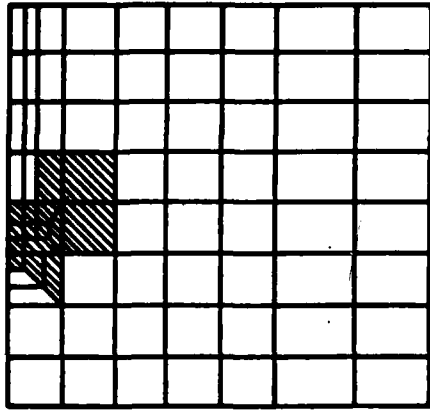
Damage Zone



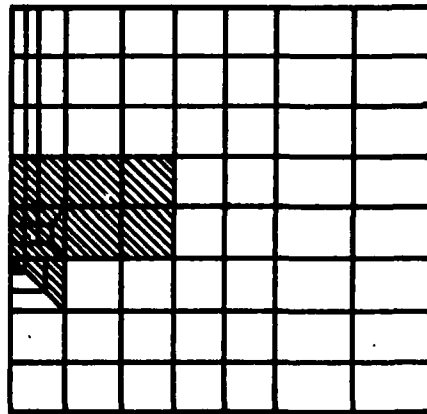
$P = 15.7 \times 10^4 \text{ lbs}$



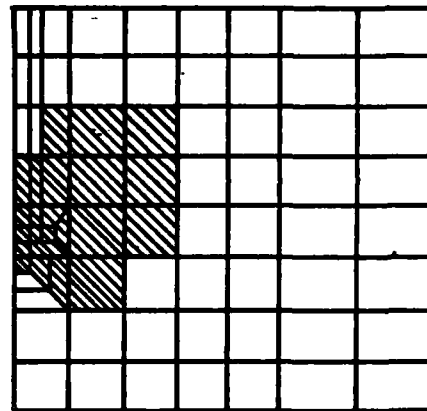
$P = 17.6 \times 10^4 \text{ lbs}$



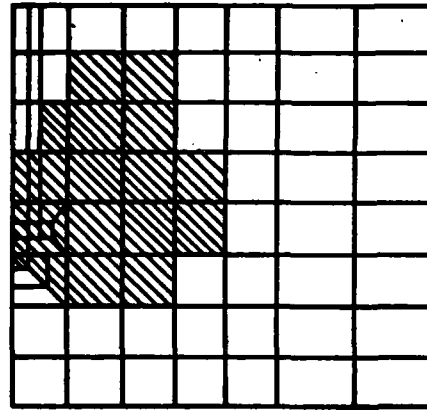
$P = 19.8 \times 10^4 \text{ lbs}$



$P = 20.6 \times 10^4 \text{ lbs}$



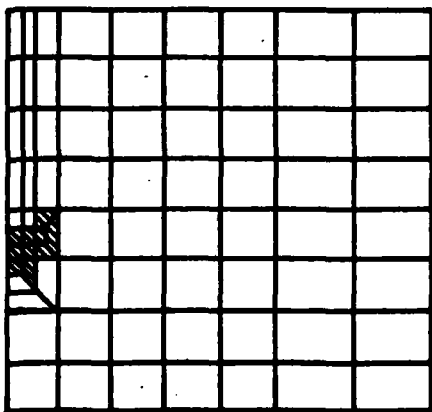
$P = 22.9 \times 10^4 \text{ lbs}$



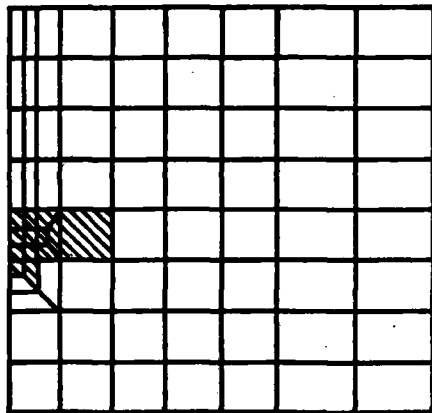
$P = 24.9 \times 10^4 \text{ lbs}$

Figure 13 - Single damage level model No. 1 damage zone development at applied load P

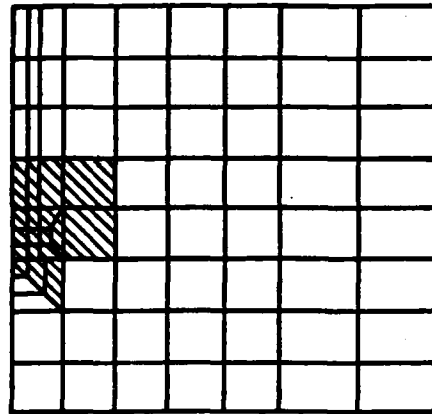
Damage Zone



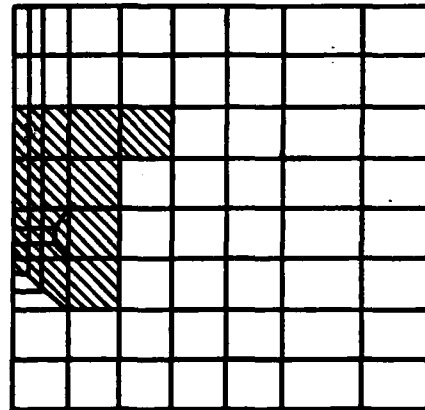
$P = 14.3 \times 10^4 \text{ lbs}$



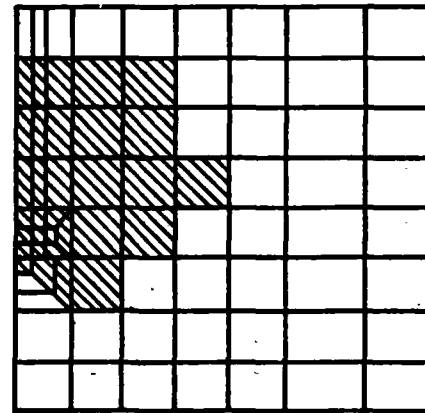
$P = 16.2 \times 10^4 \text{ lbs}$



$P = 17.7 \times 10^4 \text{ lbs}$

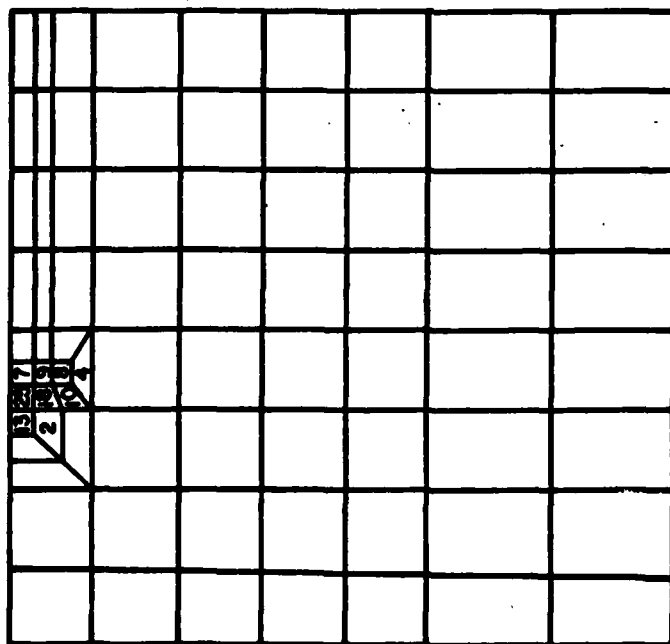


$P = 19.7 \times 10^4 \text{ lbs}$

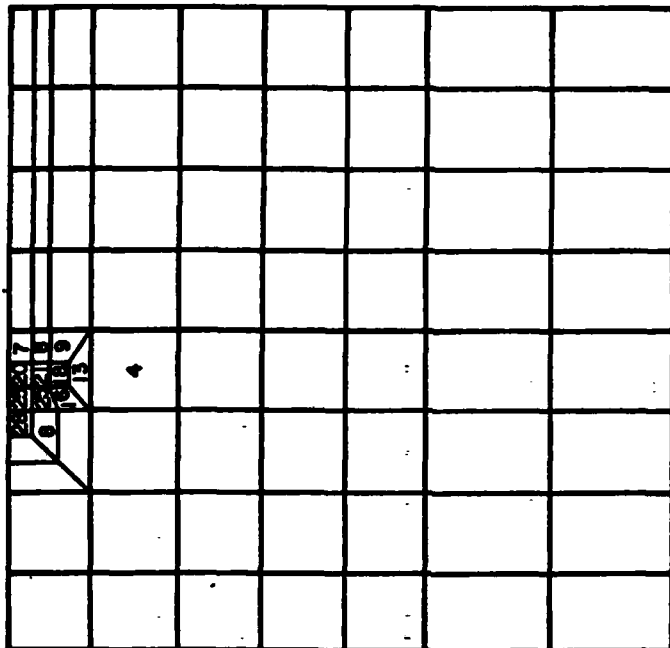


$P = 21.8 \times 10^4 \text{ lbs}$

Figure 14 - Single damage level model No. 2 damage zone development at applied load P

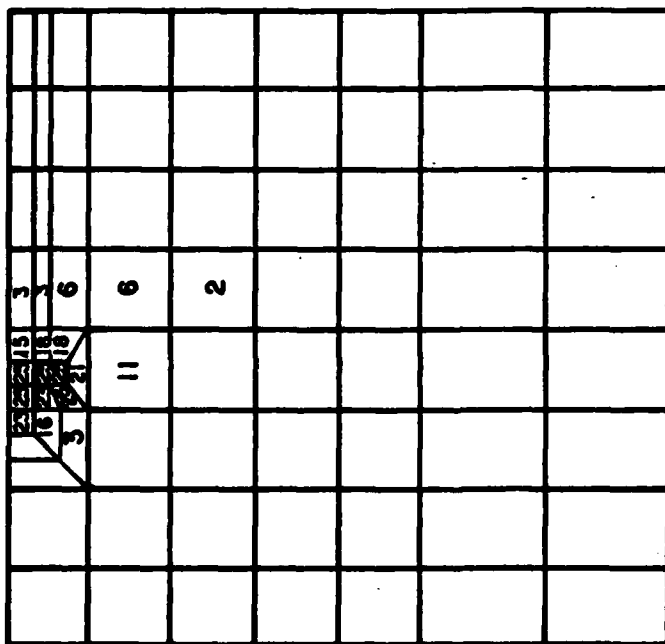


$P = 14.4 \times 10^4 \text{ lbs}$

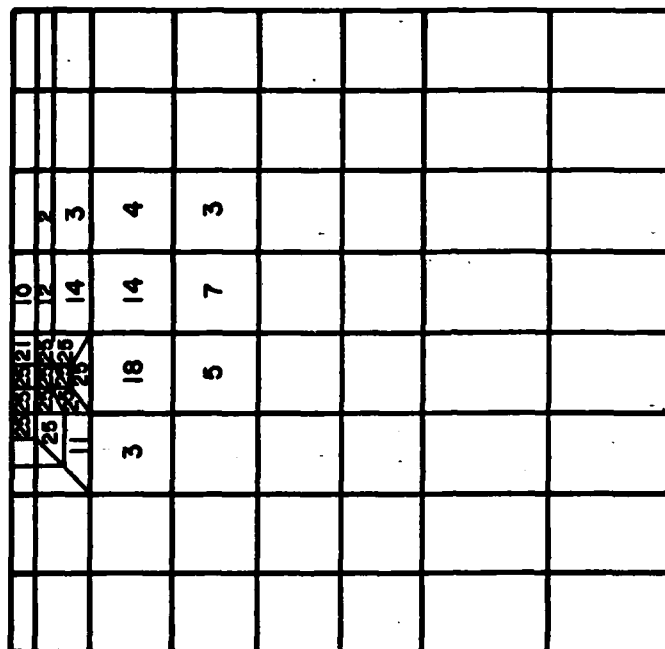


$P = 16.8 \times 10^4 \text{ lbs}$
 blank = MAT No. 1 (UNDAMAGED)

Figure 15 - Multiple damage level model damage zone at applied load P



$P = 19.2 \times 10^4 \text{ lbs}$



$P = 21.6 \times 10^4 \text{ lbs}$

blank \equiv MAT No. 1 (UNDAMAGED)

Figure 15 (continued) - Multiple damage level model damage zone at applied load P

ligament length, is probably the primary cause of the decreased global stiffness of the second case. Thus, higher damage levels in the enclaves on each side of the crack tip tend to enhance the strain energy density field ahead of the crack tip. This produces damage ahead of the crack at lower applied loads. For lower levels of damage, this effect seems to be reduced, preserving the undamaged ligament at higher applied loads.

Despite the differences in damage zone propagation, the damage center loci (Figure 16) show interesting similarities. The shape of all three loci are basically the same. Initially, for loads less than 1.8×10^5 pounds, the damage center follows the direction $\theta_0 = 1-2\nu$ of maximum strain density in the neighborhood of the crack tip, as discussed by Sih [13] for a linear elastic body. At higher values of the applied load, the damage center begins to move toward the free surface ahead of the crack tip. This seems to indicate that the effect manifests itself at a particular load, independent of the specifics of the damage models being used. This movement of the damage center may be significant in relation to the onset of macrocrack growth. It may be produced as a result of the damage zone size and geometry itself, the influence of the free surface ahead of the crack tip, or a combination of the above.

The mean secant elastic modulus (Figure 12) remains relatively constant with respect to the applied load for the Multiple Damage Level model. (This is, of course, by definition the case for the Single Damage Level model). Thus, the net increases in damage at higher loads near the crack tip are offset, in the averaging process, by the comparatively lower damage levels developing in the peripheral areas of the damage zone.

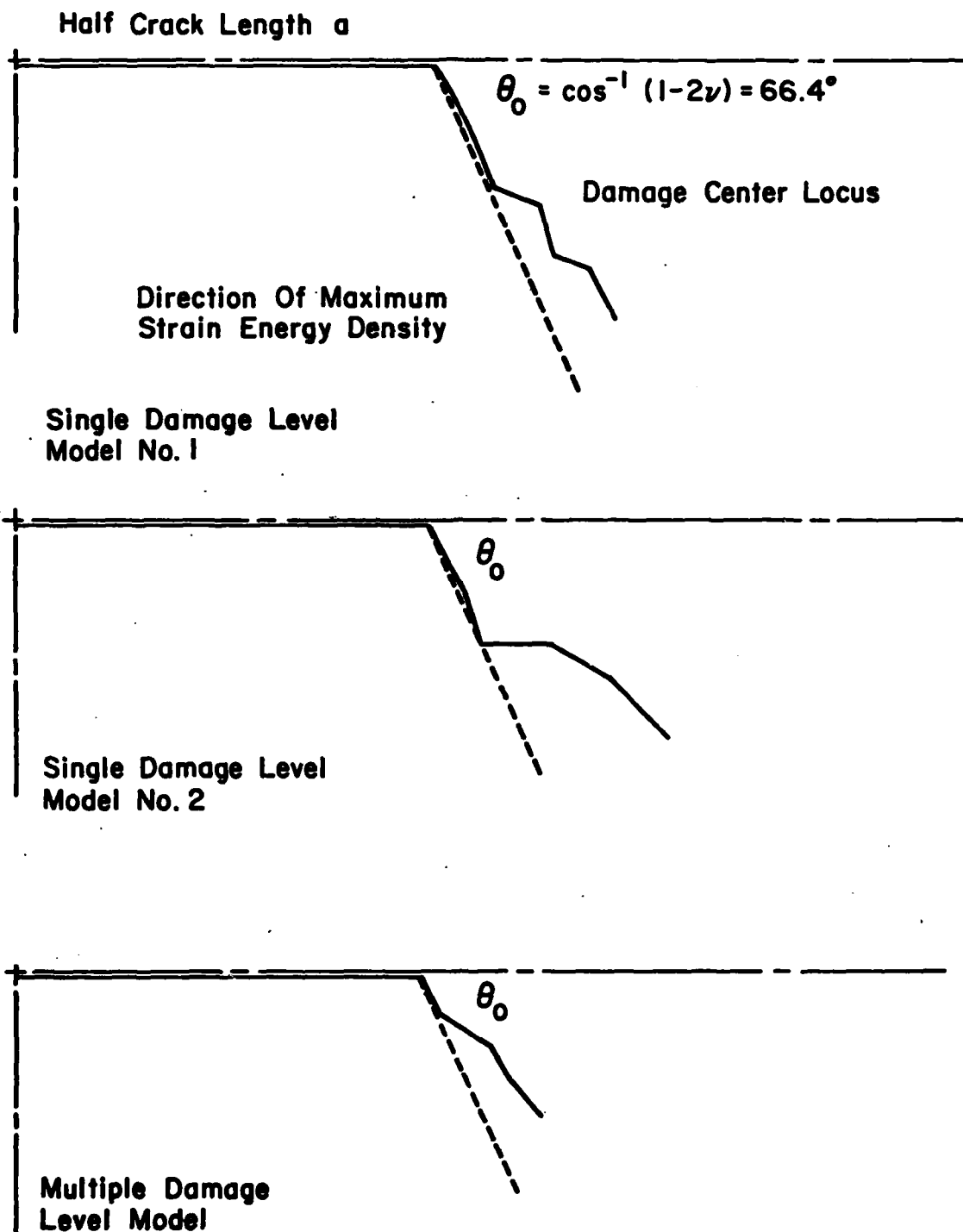


Figure 16 - Damage center loci

The suppression of macrocrack growth as applied in these analyses undoubtedly has an effect on the damage zone development in the panel. However, the consideration of this artificially constrained situation is essential in order to separate and explain the combined phenomena of micro and macro damage propagation in the panel specimen. The use of strain energy density in the criterion, as applied here, describes the level of damage in the material around the crack tip. It can be applied with consistency to the propagation of the macrocrack itself, in accordance with the theory presented by Sih [12,13], thus unifying the criteria for irreversible processes, of the types considered, at two different scale levels. It should be recalled that the microcracks in reality are accompanied by microplasticity in the sense of dislocation movement and the development of slip lines near the microcrack tips. This dissipative mechanism has not been included, thus keeping the problem elastic between each damage or load increment, and dissipation only in the sense of microcrack formation (with macrocrack extension treated in the second part of this work). This is in contrast to the more common approach of using the von Mises criteria of classical plasticity theory to describe the size and shape of the plastic zone around the crack, and a separate crack propagation criteria based on either a maximum stress component, strain component or stress intensity factor.

CONCLUDING REMARKS

The application of two different damage accumulation models, based on the strain energy density level in the material at the continuum scale, has been used to generate the global load-displacement curves for a center cracked panel in the absence of macrocrack propagation. These models have qualitatively shown how such a criterion has the potential to be interpreted in terms of a specific damage mechanism at, or below, the continuum scale. Further investigation should address the details of these damage mechanisms and the way in which they influence the effective material properties of the material. This, in turn, would lead to improved damage accumulation models and a better understanding of the effects material damage has on the behavior of structural members.

Damage models which incorporate two or more mechanisms undoubtedly would result in a more complete formulation of the problem. The details of initiation and propagation processes of microcracks will provide insight into the energy dissipating processes which occur at this scale. With this information, the tensile test specimen dimensions may be specifically chosen on the basis of the damage processes which the specimen seeks to reflect. The continuum properties obtained from the specimen's true stress-true strain curve will then correspond to the processes that are actually occurring in a structural member. The appropriate choice of variables, which will be capable of describing the state of damage in the material, can then be incorporated into the constitutive relations for the material. These relations will directly relate material damage at the continuum scale to the global behavior of a structural member.

BIBLIOGRAPHY

- [1] Budiansky, B. and O'Connell, R. J., "Elastic Moduli of a Cracked Solid", Int. J. Solids Structures, 12, pp. 81-97, 1976.
- [2] Delameter, W. R., Herrmann, G. and Barnett, D. M., "Weakening of an Elastic Solid by a Rectangular Array of Cracks", Jnl. of Applied Mechanics 42, pp. 74-80, 1975 and 44, p. 190, 1977.
- [3] Eimer, C., "Elasticity of Cracked Medium", Archives of Mechanics 30, pp. 827-836, 1978.
- [4] Eimer, C., "Bulk Properties of Cracked Medium", Proc. of Cont. on Continuum Models of Discrete Systems, pp. 819-835, 1979.
- [5] Eimer, C., "Bulk Constitutive Relations for Cracked Materials", Archives of Mechanics 31, pp. 519-532, 1979.
- [6] Eshelby, J. D., "The Determination of the Elastic Field of an Ellipsoidal Inclusion, and Related Problems", Proc. Royal Soc. A241, pp. 376-396, 1957.
- [7] Gottesman, T., Hashin, Z. and Brull, M. A., "Effective Elastic Properties of Cracked Materials", Office of Naval Research, Contract N00014-78-C-0544, Technical Report No. 6, May 1981.
- [8] Hilton, P. D., Gifford, L. N. and Lomacky, O., "Finite Element Fracture Mechanics of Two Dimensional and Axisymmetric Elastic and Elastic-Plastic Cracked Structures", Naval Ship Research and Development Center Report No. 4493, 1975.

- [9] Hilton, P. D. and Hutchinson, J. W., "Plastic Intensity Factors for Cracked Plates", Engng. Fracture Mech., 3, pp. 435-451, 1971.
- [10] Hoenig, A., "Elastic Moduli of a Non-Randomly Cracked Body", Int. J. Solids Structures 15, pp. 137-154, 1979.
- [11] Hoenig, A., "The Behavior of a Flat Elliptical Crack in an Anisotropic Elastic Body", Int. J. Solids Structures 14, pp. 925-934, 1978.
- [12] Sih, G. C. and MacDonald, B., "Fracture Mechanics Applied to Engineering Problems - Strain Energy Density Fracture Criterion", Engng. Fracture Mech., 6, pp. 361-368, 1974.
- [13] Sih, G. C., "A Special Theory of Crack Propagation", Methods of Analysis and Solution of Crack Problems", (Ed. G. C. Sih), pp. XXI-XLV, Noordhoff, Leyden, 1973.

APPENDIX A - DISCUSSION OF UPPER AND LOWER BOUNDS OF GENERATED
LOAD DISPLACEMENT CURVES

In the Single Damage Level Model, the sequence in which the finite elements of the center cracked panel specimen fail is unique, since the value of the strain energy density in each element is the result of a unique stress field. When multiple element failure is used to generate the damage increment in this model, the question arises as to how much of a damage increment can be introduced while still producing a physically realistic load-displacement curve. Discussion of reasonable upper and lower bounding procedures is included here for this purpose.

Consider the m th portion of the generated load displacement curve (Figure A1.1) for the center cracked panel with a stiffness S_m . Prior to accumulating the damage resulting in this stiffness, which occurred at an applied load of P_{m-1} , the stiffness of the panel was S_{m-1} for the $m-1$ segment of the curve. Note that in the context of the pseudo-linear elastic material formulation used in the damage model, all portions of the load-displacement curve (except those corresponding to the damage increment) extrapolate back to the origin of the $P-\delta$ axes. Regressing further along the curve another increment yields the $m-2$ segment, with local stiffness S_{m-2} and the applied load P_{m-2} .

Define the tangent stiffness S_m^t as the slope of the line passing through the points on the incremental curve labelled "A" and "B". Thus,

$$S_m^t = \frac{P_{m-1} - P_{m-2}}{\delta_B - \delta_A} \quad (A1)$$

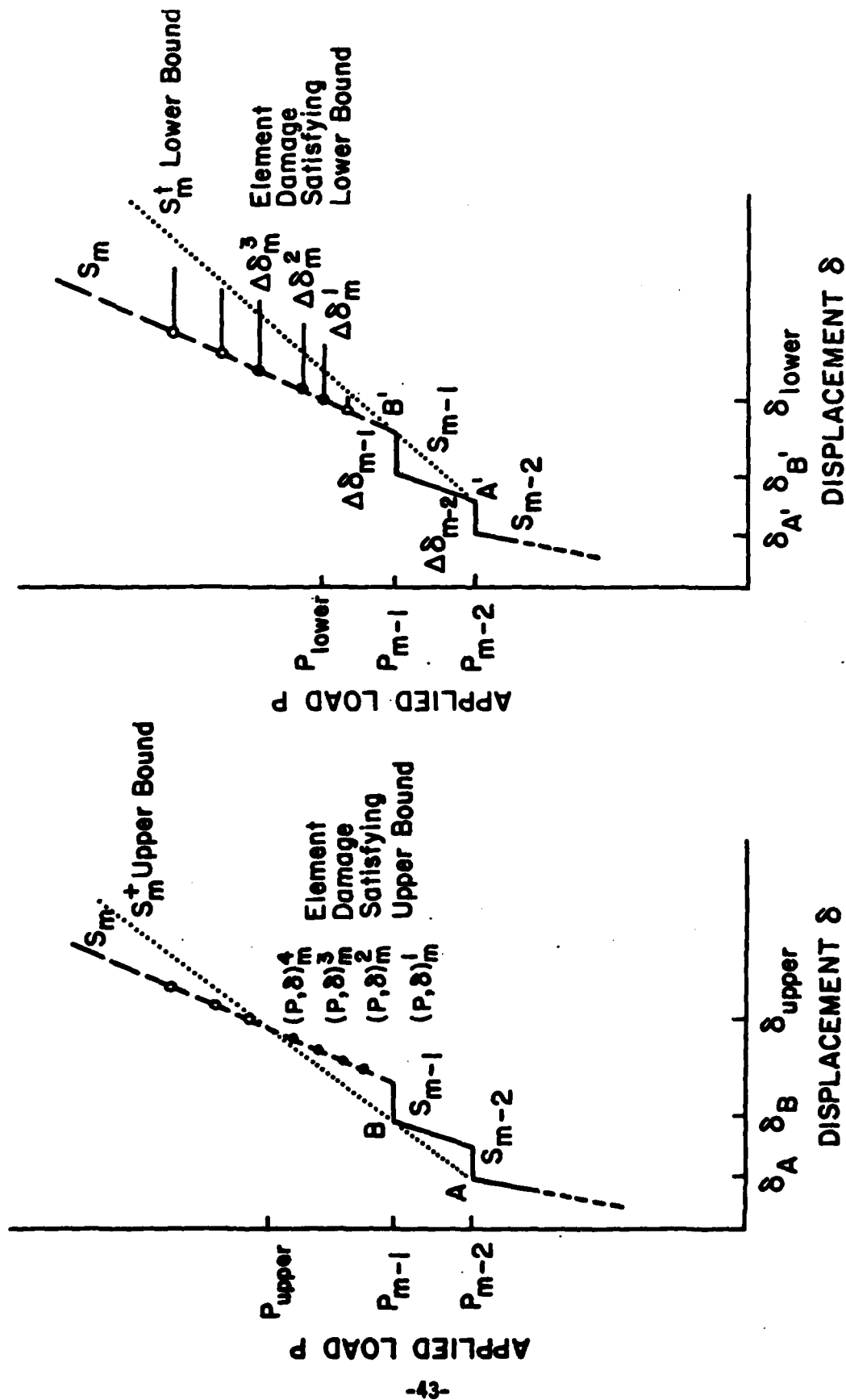


Figure A1.1 - Upper and lower bounds for load and displacement increments

This is, of course, simply an approximation to the actual tangent stiffness, $\partial P / \partial \delta$.

From the physical behavior of a center cracked panel made of a ductile material, in the absence of crack propagation, one would expect a smooth load-displacement curve to develop. The slope of the curve should remain constant or decrease, implying

$$\frac{\partial S_m^t}{\partial \delta} = \frac{\partial}{\partial \delta} \left(\frac{\partial P}{\partial \delta} \right) \leq 0 \quad (A2)$$

This condition, as applied to the incremental load displacement curve through the value of S_m^t , sets an upper bound to the applied load P_m .

Denote by a dark circle "•" those $(P, \delta)_j$ points on the m th local stiffness curve where the j th element will fail. These elements are below the upper bound set by the intersection of the S_m^t and the S_m lines which define an upper bound applied load P_{upper} . All other elements, labelled with an open circle "o", which have not accumulated damage at an applied load less than or equal to P_{m-1} must lie on the secant modulus line at points corresponding to loads P_j which lie above P_{upper} . Failure of any of these elements would produce a physically unrealistic load-displacement curve.

Alternately, a tangent stiffness S_m^t may be defined as the slope of the line passing through the points A' and B' on the incremental load-displacement curve (Figure A1.2). In this case

$$S_m^t = \frac{P_{m-1} - P_{m-2}}{\delta_{B'} - \delta_{A'}} \quad (A3)$$

This, also, is an approximation to the actual tangent stiffness, $\partial P / \partial S$.

If the physical behavior of the center cracked panel is considered, it should be clear that due to identical reasons as discussed above,

$$\frac{\partial S^t}{\partial \delta} = \frac{\partial}{\partial \delta} \left(\frac{\partial P}{\partial S} \right) \leq 0 \quad (A4)$$

i.e., the tangent modulus should not increase with increasing load. This condition will be satisfied if the n th damage increment produces a displacement increment $\Delta \delta_m$ such that the displacement subsequent to the damage accumulation increment is greater than that defined by the tangent stiffness line. The failure of an undamaged element, (along with those undamaged elements having a higher strain energy density for the applied failure load), is denoted by a dark circle "e". On the m th local stiffness curve, this defines the groups of elements which satisfy this lower bound by producing a sufficiently large displacement increment $\Delta \delta_m$. The other undamaged elements, labelled with an open circle "o", define those sets of damaged elements which would not satisfy the lower bound since an insufficient displacement increment $\Delta \delta_m$ would be produced.

In the case of the Multiple Damage Level model, the same approach is used with the following difference. The load increment is the independent variable, requiring that any load P_m satisfying the condition $P_{m-1} \leq P_m \leq P_{upper}$ satisfies the upper bound. The resulting damage increment $\Delta \delta_m$ must in turn satisfy the lower bound.

In application, it should be noted that the upper bound can be used to insure that the applied load P_{upper} is not surpassed in choosing the damage increment. The lower bound, however, can only be used to check on the choice of the applied

load P_m , since the displacement increment must be calculated in order to be compared with the lower bound tangent stiffness line.

APPENDIX 2.1 - SINGLE DAMAGE LEVEL MODEL NO. 1 ELEMENT DAMAGE SEQUENCE

		Element Damage Sequence (First → Last)									
Damage Increment	No. 1	56	57	55	66	72	58	60	59	53	61
	No. 2	67	73	44							
	No. 3	45	62	52							
	No. 4	68	74	36	37						
	No. 5	43	46	63	38						

APPENDIX 2.2 - SINGLE DAMAGE LEVEL MODEL NO. 2 ELEMENT DAMAGE SEQUENCE

		Element Damage Sequence (First → Last)									
Damage Increment	No. 1	56	57	55	66	72	58	60	59	53	61
	No. 2	67	73	44							
	No. 3	62	45	68	74	52					
	No. 4	63	46	69	75	38	43				
	No. 5	37	36	47	64	70	76	39	29		

APPENDIX 2.3 - MULTIPLE DAMAGE LEVEL MODEL ELEMENT DAMAGE LEVEL PRODUCED BY APPLIED LOAD P

	P = 14.4 x 10 ³ lbs	P = 16.8 x 10 ³ lbs	P = 19.2 x 10 ³ lbs	P = 21.6 x 10 ³ lbs
36				5
37			2	7
38				3
43				3
44		4	11	18
45			6	14
46				4
52			3	11
53	2	8	16	25
55	13	23	25	25
56	25	25	25	25
57	18	25	25	25
58	10	16	25	25
59	4	13	21	25
60	8	18	25	25
61		9	18	25
62			6	14
63				3
66	9	21	25	25
67		9	18	25
68			5	12
69				2
72	7	20	25	25
73		7	15	21
74			3	10

Element Number

AIR FORCE OFFICE OF SCIENTIFIC RESEARCH
DISTRIBUTION LIST
SOLID MECHANICS

Dr. John C. Houbolt
Aeronautical Research Associates
of Princeton, Inc.
50 Washington Road
Princeton, NJ 08540

Dr. John E. Yates
Aeronautical Research Associates
of Princeton, Inc.
50 Washington Road
Princeton, NJ 08540

Mr. Bernard Mazelsky
Aerospace Research Associates
2017 W. Garvey Avenue
West Covina, CA 91790

Professor Joseph Kempner
Polytechnic Institute of Brooklyn
Department of Applied Mechanics
333 Jay Street
Brooklyn, NY 11201

Dr. M. A. Biot
Avenue Paul Hymans 117
B-1200 Bruxelles, Belgium

Professor C. D. Babcock
California Institute of Technology
Graduate Aeronautical Laboratories
Pasadena, CA 91109

Professor W. Nachbar
University of California, San Diego
Department of Aerospace & Mechanical
Engineering Sciences
La Jolla, CA 92037

Professors A. T. Ellis &
G. A. Hegemier
University of California, San Diego
Department of Applied Mechanics &
Engineering Sciences
La Jolla, CA 92037

Professor L. J. Ebert
Case Western Reserve University
Department of Metallurgy
University Circle
Cleveland, OH 44106

Professor A. J. McEvily, Jr.
The University of Connecticut
Department of Metallurgy &
Physics
Storrs, CT 06268

Professor I. G. Greenfield
University of Delaware
Department of Mechanical &
Aerospace Engineering
Newark, DE 19711

Professor J. R. Vinson
University of Delaware
Department of Mechanical &
Aerospace Engineering
Newark, DE 19711

Professor J. L. Rose
Drexel University
Department of Mechanical
Engineering
Philadelphia, PA 19104

Dr. L. W. Rehfield
Georgia Institute of Technology
School of Aerospace Engineering
Atlanta, GA 30332

Professor Lawrence J. Broutman
Illinois Institute of Technology
Department of Metallurgical
Engineering
Chicago, IL 60616

Professors R. E. Green &
R. B. Pond, Sr.
The Johns Hopkins University
Department of Mechanics
Baltimore, MD 21218

Dr. George C. M. Sih
Lehigh University
Department of Mechanics
Bethlehem, PA 18015

Dr. I. R. Kramer
The Martin Company
Denver Division
Denver, CO 80201

Professor T. H. E. Pian
Massachusetts Institute of
Technology
Department of Aeronautics &
Astronautics
Cambridge, MA 02139

Professor E. Crowan
Massachusetts Institute of
Technology
Department of Mechanical
Engineering
Cambridge, MA 02139

Professor James W. Mar
Massachusetts Institute of
Technology
Department of Aeronautical &
Astronautical Engineering
Cambridge, MA 02139

Professor William A. Nash
The University of Massachusetts
Department of Mechanical &
Aerospace Engineering
Amherst, MA 01003

Dr. J. R. Hancock
Midwest Research Institute
Materials Science Section
Kansas City, MO 64110

Professor Herbert Reismann
State University of New York
at Buffalo
Karr Parker Engineering Building
Chemistry Road
Buffalo, NY 14214

Professor Arnold D. Kerr
Department of Aeronautics &
Astronautics
University Heights
Bronx, NY 10453

Professor J. Kiusalaas
The Pennsylvania State University
Department of Engineering
Mechanics
University Park, PA 16802

Dr. M. J. Salkind
Sikorsky Aircraft
Stratford, CT 06602

Dr. R. M. Jones
Southern Methodist University
Solid Mechanics Center
Dallas, TX 75222

Dr. U. S. Lindholm
Southwest Research Institute
8500 Culebra Road
San Antonio, TX 78206

Mr. J. R. Barton
Southwest Research Institute
8500 Culebra Road
San Antonio, TX 78206

Professor George Herrmann
Stanford University
Department of Applied Mechanics
& Civil Engineering
Stanford, CA 94305

Professor Josef Singer
Technion-Israel Institute of
Technology
Department of Aeronautical
Engineering
Haifa, Israel

Professor Sol R. Bodner
Technion-Israel Institute of
Technology
Department of Materials
Engineering
Haifa, Israel

Professor M. Baruch
Technion-Israel Institute of
Technology
Department of Aeronautical
Engineering
Haifa, Israel

Professor Zvi Hashin
Technion-Israel Institute of
Technology
Department of Materials
Engineering
Haifa, Israel

Professor Moche Ziv
Technion-Israel Institute of
Technology
Department of Aeronautical
Engineering
Haifa, Israel

Professor Y. Weitsman
Tel Aviv University
Department of Engineering Sciences
Tel Aviv, Israel

Dr. R. O. Stearman
The University of Texas
Department of Aerospace
Engineering
Austin, TX 78712

Professor J. Tinsley Oden
The University of Texas
Department of Aerospace
Engineering & Engineering
Mechanics
Austin, TX 78712

Professors C. V. B. Gowda &
T. H. Topper
University of Waterloo
Department of Civil Engineering
Waterloo, Ontario, Canada

Professor Paul F. Packman
Vanderbilt University
Department of Materials Science
& Engineering
Nashville, TN 37235

Professor K. Reifsnider
Virginia Polytechnic Institute
& State University
Department of Engineering
Mechanics
Blacksburg, VA 24061

Drs. S. Atluri & A. S.
Kobayashi
University of Washington
Department of Aeronautics &
Astronautics
Seattle, WA 98195

Dr. Harold Liebowitz
The George Washington University
School of Engineering & Applied
Science
727 23rd Street NW
Washington, DC 20006

Grumman Aircraft Engineering
Corporation
Attn: Library
Bethpage, LI, NY 11714

Dr. Leonard Mordfin
National Bureau of Standards
Room EN 219
Washington, DC 20234

Army Research Office
Attn: George Mayer & Jim
Murray
Box CM, Duke Station
Durham, NC 27706

AFFDL/FBC/Mr. G. P. Sendeckyj
Wright-Patterson AFB OH 45433

AFFDL/FY/Mr. Mykytow
Wright-Patterson AFB OH 45433

AFFDL/FB-1/Mr. Collier
Wright-Patterson AFB OH 45433

AFFDL/FBR/Mr. Bader
Wright-Patterson AFB OH 45433

AFML/LNC/Dr. Nick Pagano
Wright-Patterson AFB OH 45433

AFML/MBM/Dr. S. W. Tsai
Wright-Patterson AFB OH 45433

Dr. S. B. Batdorf
Aerospace Corporation
P. O. Box 95085
Los Angeles, CA 90045

Professor A. S. Shreeve, Jr.
University of Maryland
Head, Department of Mechanical
Engineering
College Park, MD 20742

The Boeing Company
Attn: Aerospace Group Library
P. O. Box 3999
Seattle, WA 98124

Ling-Temco Vought Research
Center
Attn: Library
Dallas, TX

McDonnell Douglas Corporation
P. O. Box 516
St. Louis, MO 63166
Attn: McDonnell Library Dept.
218 Ref # 69LI 351

ATE
MED
8